1969

Experiments on restrained columns permitted to sway june 1970

S. W. Kim

J. H. Daniels

L. W. Lu

Strength of Beam-and-Column Subassemblages in
Unbraced Multi-Story Frames

EXPERIMENTS ON RESTRAINED COLUMNS PERMITTED TO SWAY

by

S. W. Kim

J. Hartley Daniels

This work has been carried out as part of an investigation by the American Iron and Steel Institute.

Department of Civil Engineering

Fritz Engineering Laboratory

Lehigh University

Bethlehem, Pennsylvania

June 1970

Fritz Engineering Laboratory Report No. 346.3

SYNOPSIS

Experiments were conducted on full-scale restrained columns permitted to sway in order to study their lateral-load versus sway-deflection behavior with a variable rotational restraint stiffness. These tests also provided experimental verification of some aspects of the sway subassemblage method of analysis. Three restrained columns were tested, simulating the restrained columns in a windward, an interior and a leeward sway subassemblage. The column axial load ratio for all the restrained columns was maintained constant at 0.7. Each test specimen consisted of one column and one or two restraining beams welded to the column. The rotational restraint stiffness of restrained column varied during the test due to the formation of a plastic hinge. The test results show good agreement with the predictions from restrained column theory.

TABLE OF CONTENTS

1. INTRODUCTION

The sway subassemblage method of analysis was developed to study the behavior of a single story of an unbraced frame which is subjected to combined gravity and lateral loads.[1,2,3] In the method, a one-story assemblage is isolated from the frame by cutting the columns at the points of inflection which are assumed to be located at mid-height of the story. This is equivalent to assuming that the columns in these stories are bent into symmetrical double curvature.

A typical one-story assemblage of story height h and at level n is shown in Fig. 1(a), together with the member forces and the resulting deformations. The applied shear above level n is ΣH_{n-1} and is computed as the sum of the known lateral forces acting on the frame above level n. Similarly the applied shear below level n is ΣH_n where $\Sigma H_n = \Sigma H_{n-1} + H_n$. The constants λ_A, λ_B and λ_C define the distribution of the applied shear to each column and are assumed to be the same above and below level n. The axial forces P_{n-1} and P_n and the distributed beam loads w are calculated from the known frame loads.

In the sway subassemblage method the one-story assemblage is further sub-divided into sway subassemblages as shown in Fig. 1(b). Each sway subassemblage consists of a restrained column, which is permitted to sway, together with the adjacent restraining beams.

A spring at each end of the restraining beams represents the rotational restraint offered by the members outside a sway subassemblage. The columns above level n are replaced by the equivalent joint forces where, conservatively it is assumed that $\Sigma H_{n-1} = \Sigma H_n$. The behavior of a sway subassemblage is then described by the behavior of a restrained column at level n, which is subjected to the forces shown in Fig. 2. The behavior of this restrained column can be determined either manually with the aid of prepared curves, or by computer.[1,4,5,6] The behavior of the one-story assemblage is determined by suitably combining the individual behavior of the restrained columns, or the sway subassemblages.[1]

A numerical method of analysis for restrained columns having any type of rotational and lateral restraints and subjected to any combination of external moments and forces was first presented by Levi.[7] The restrained column shown in Fig. 2 is a special case of the general restrained column problem. This column, of height h/2, is pinned at the lower end, and subjected at the upper end to constant axial load P_n, variable lateral load Q_n, variable joint moment M_n and a restraining moment which is a function of a variable rotational restraint stiffness k. The variation of the rotational restraint stiffness results from the formation of plastic hinges in the restraining beams.

The purpose of this report is to present the results of an experimental investigation of three restrained columns permitted to sway. In two tests, a variable restraint stiffness was obtained by ensuring that a plastic hinge developed in the restraining beam before the attainment of the stability limit load. The ex-

perimental results from each test are compared with the predictions provided by restrained column theory.

2. EXPERIMENT DESIGN

Each test specimen consisted of one or two restraining beams welded to a column as shown in Fig. 3. The restrained column (lower half of each column in Fig. 3) in each test specimen was designed to represent a restrained column in either a windward, an interior, or a leeward sway subassemblage (See Fig. 1(b)). In order to provide more or less realistic geometry, rotational restraint stiffness and column slenderness ratios, the test specimens were designed to represent part of a one-story assemblage with two 15-ft bays and a 10-ft story height. A column slenderness ratio of approximately 40 for all three specimens was chosen to represent the maximum slenderness ratio found in the middle and lower stories of an unbraced frame. An 8W40 section was selected for all columns and a 12B22 section for all beams. The ratio of strong axis moments of inertia for the sections is also typical of that found in the middle and lower stories of an unbraced frame. The dimensions of the three specimens, RC-1, RC-2 and RC-3, are shown in Fig. 3.

In the actual tests, it would be very difficult to provide the rotational restraint at the free end of a restraining beam, as required by sway subassemblage theory. Therefore, it was decided to test restrained columns with pin ended restraining beams.[8] In effect, these restrained column tests would also be the tests of sway subassemblages after a plastic hinge has formed at the far end of a restraining beam. The results of the restrained column tests

could be extrapolated to predict the experimental behavior of sway subassemblages with realistic boundary conditions imposed.

In order to obtain considerable plastification of the columns and to explore the effect of column residual stresses on the experimental results, it was decided to use a high value of the column axial load ratio P/P_y, where P is the applied column load and P_y the yield load. The axial load ratio for each restrained column was arbitrarily chosen as 0.7. No attempt was made to relate the experiment design to a set of probable working loads, load factors and bent spacings for a frame containing the assumed one-story assemblage mentioned before. An analysis of the restrained columns indicated that the variation in the axial load ratio for each restrained column during testing would be insignificant. It was therefore decided that the vertical column load which was computed to give an axial load ratio of 0.7 at the start of each test would be maintained constant throughout the test.

The vertical beam loads were applied approximately at the quarter points in order to accommodate the available gravity load simulators.[9] These loads were to be maintained constant and at magnitudes that would ensure the formation of plastic hinges at the desired locations as follows: For specimen RC-1, a plastic hinge was designed to occur in the restraining beam under the load point nearest the column is shown in Fig. 4. For RC-2, the first plastic hinge was designed to occur in the restraining beam at the column face with the second plastic hinge at the top of the restrained column. The plastic hinge in RC-3 was designed to form at the top

of the restrained column. The constant values of vertical column and beam loads are shown in Fig. 4. These values were determined on the basis of the measured yield stress level of the materials.

Each restrained column was designed to be displaced during testing in the direction shown in Fig. 4. The primary behavior to be determined from each test was the relationship between the resulting lateral force Q at the top of the upper column and the lateral displacement $\Delta/2$ at the top of the restrained column (joint). In the zero-sway position an initial value of horizontal load Q was required to maintain equilibrium of the test specimen. For specimen RC-1 Q was initially -5.68 kips. For specimen RC-3 Q was initially + 5.68 kips. Due to symmetry of geometry and loading, no initial horizontal load was required for RC-2.

3. CONTROL TESTS

A number of control tests were performed on the materials used for the test specimens. The purpose of these control tests was to determine the material properties and geometry of the sections used.

3.1 Tensile Coupon Tests

ASTM A36 rolled steel was used for all test specimens. The chemical composition and mill test results, as furnished by the manufacturer, are given in Table 1. Nine tensile coupons, 5 from the flanges and 4 from the web, were tested from the 12B22 beam section. For the 8W40 column section, eight tension tests, (5 from flanges and 3 from web) were performed. The average of the flange and web static yield stress levels for each section are given in Table 2, along with the ultimate stress attained and the percent elongations.

3.2 Residual Stress Measurement

One residual strain measurement was performed on the 8W40 section used for the columns of the test specimens. The residual stresses were determined by the method of sectioning. The calculated residual stresses are shown in Fig. 5. The average residual stress at the flange tips was 7.5 ksi or 0.23 σ_y. The residual stress distribution obtained was typical for cross-section which are cold-straightened by gagging.

3.3 Stub Column Test

One stub column test was performed on the 8W40 section to determine the axial yield load, P_y. The load-deformation relationship obtained in the test is given in Fig. 6. The value of P_y obtained from the stub column test was about 370 kips, which resulted in an average static yield stress of 32.1 ksi. The value of P_y calculated from the measured cross-sectional area of the section (Section 3.4) and yield stress levels of the flanges and web shown in Table 2 was 367 kips. The two values of P_y are in very good agreement. For all the theoretical computations, the calculated value of P_y (367 kips) was used.

3.4 Cross-Section Measurement

The cross-section dimensions of each shape were measured at various locations along the length of each beam and column using micrometers and calipers. Measurements of web thickness were taken only at the cut ends of each length. The average measured sectional properties are given in Table 3, and compared with the corresponding handbook values. There were no large differences between the measured and handbook properties. The measured values were used to determine the area, A, the moment inertia, I_x, and the plastic section modulus, Z_x, for each shape. The calculated plastic moment capacities of the 12B22 and 8W40 sections were 1020 k-in and 1240 k-in respectively. This compares with the nominal values of 1060 k-in and 1435 k-in, based on handbook properties.

4. TEST SETUP AND PROCEDURE

4.1 General

Two different types of test set ups were used, one for tests RC-1 and RC-3, and the other for test RC-2. Overall views of the test setup for RC-1 and RC-3 are shown in Figs. 7 and 8. Similarly, Figs. 9 and 10 show the test setup for test RC-2.

In both test setups, the top and the bottom ends of the columns were hinged. Figure 11 shows a typical view of the column hinge and hinge support detail used in the tests. A large roller bearing was used to ensure that there would be no bending moments at the ends of the columns.

The restraining beams were fully welded to the column flanges at one end using standard welding procedures. The other end of each beam was supported by rollers positioned on either side of the beam. The rollers were free to rotate on large roller bearings mounted on a shaft welded perpendicular to the web of the beam. Each roller was free to move horizontally in a roller guide which provided vertical support and alignment of the end of the beam. Schematic views of the rollers and roller guides are shown in Figs. 7 and 9. Figure 12 shows a typical end view of a beam together with the rollers and the roller guides. By using this beam support system, the end of a restraining beam could be moved horizontally without restraint, while maintaining the same span length, regardless of the horizontal deflection of the column.

Planar motion of each test specimen under load was ensured by means of lateral bracing perpendicular to the plane of the test specimen as shown in Fig. 13.[9] The bracing system used prevented lateral and torsional movement of the beam but did not offer restraint to in-plane deformation. The braces were placed at the locations recommended for use in plastic design.[10] Five braces were used for each beam as shown in the figure. The columns were braced using the same type of bracing members. They were located at the level of the restraining beam and at each column top. All braces were in turn attached to an independent supporting frame.

4.2 Loading

The column axial loads were applied to the top of the columns through a beam which was connected to the tension jacks of four gravity load simulators.[9] The gravity load simulators were symmetrically placed in pairs on either side of a column as shown in Fig. 14. Thus the applied column loads remained vertical throughout each test. In order to transmit the large loads from the tension jacks to the column top, a substantial loading beam was fabricated. The loading beam was mounted on the column hinge and hinge support assemblage at the top of a column. Weak axis bending was eliminated by aligning the loading beam to ensure axial distribution of the load. Four tension rods were used to connect the tension jacks of the simulators to the loading beam and were calibrated to determine the load from each jack. The four calibrated rods are also shown in Fig. 14. A common hydraulic line was connected to each of the four tension jacks to maintain as nearly as possible the same load on each jack.

Vertical loads were applied approximately at the quarter points of each restraining beam through a spreader beam which was attached at its mid-point to the tension jack of a gravity load simulator as shown in Fig. 13. Dynamometers were used to connect the spreader beam to the test specimen and also to measure the applied loads. In test RC-2, the tension jacks of two simulators which were used to apply the vertical beam loads were connected to a common hydraulic line.

The horizontal displacement of the column top was controlled by a screw jack mounted horizontally as shown in Fig. 15. The jack was pin connected to the column top through a dynamometer to measure the horizontal load applied by the jack. The jack was also pin connected to an independent supporting frame.

4.3 Instrumentation

The instrumentation used for each test set up was designed to obtain strain data which could be used to monitor the applied loads, to determine overall deformations and to calculate the internal stress resultants in each test specimen. Strains in the beams and columns were measured using SR-4 electrical resistance strain gages. Four strain gages were used at each instrumented cross-section so that the axial face and bending moment at the cross-section could be calculated. Four cross-sections were gaged on each column and six cross-sections were gaged on each beam as shown in Fig. 16.

A transit was used to measure the horizontal movements of the columns by reading scales attached to an outside face of each column at the locations shown in Fig. 16. The vertical movements of the

beams were also measured by taking level readings on scales positioned as shown in Fig. 16. In addition to the direct readings from scales, electrical displacement gages were also used to measure the vertical and horizontal displacements of the beams and columns. A typical electrical displacement gage used in the tests is shown in Fig. 17(c).

Rotations were measured using both electrical and mechanical rotation gages as shown in Figs. 17(a) and (b). Electrical rotation gages were placed at the top and bottom of each column, at the beam-to-column connections, at locations of potential plastic hinges and at the exterior end of each beam. Mechanical rotation gages were placed at the top and bottom of each column and at the exterior end of each beam to check the readings from the electrical rotation gages at those locations. The locations of rotational gages are also shown in Fig. 16.

Each test specimen was whitewashed prior to testing in order to observe the progression of yielding. All readings from SR-4 strain gages, electrical rotation gages and electrical displacement gages were read by a multi-channel strain gage recording system and punched automatically onto computer cards. This procedure allows a systematic data reduction to be performed later using a computer program.

4.4 Alignment Procedure

Each column was first placed on its pin-base support (Fig. 11) and aligned with a transit to ensure that it was plumb. Each restraining beam was also aligned with a plumb line and a carpenter's level to ensure that it was in the correct position. The roller

guides at the exterior end of each beam were also aligned so that they were parallel to the beam and horizontal. After all alignment was complete each beam was welded to the column. Then all lateral braces were attached.

After setting up each test specimen, it was necessary to adjust the loading beam at the column top to eliminate the eccentricity of the axial load. Using standard stub-column test procedures strain readings were taken at several load levels. Based on the strain readings which were obtained, the position of the loading beam was adjusted to reduce the eccentricity of load. The tests did not proceed until the column load was applied with negligible eccentricity.

4.5 Test Procedure

At the start of each test, one half of the design column load and the design beam loads were simultaneously applied. The column load was then gradually increased to its full load while the beam loads were held constant. The resulting column and beam loads were maintained constant throughout each test. Before beginning each test but after all vertical loads had been applied the restrained column was plumbed by making a small in-plane displacement of the column top in order to reduce the deflection $\Delta/2$ at the center of the joint to zero. The lateral load at the column top required to maintain the test frame in this position was then recorded. This lateral load in addition to the vertical column and beam loads previously applied were as the initial test loads corresponding to zero lateral displacement of the restrained column. From this initial point the displacement $\Delta/2$ of the joint was incremented using the horizontal jack at the column top. In test RC-1, the horizontal deflection of the joint was incremented

in approximately 0.1 in. intervals. Approximately 0.05 in. increments were used for RC-2 and RC-3. Readings of all the strain gages, dynamometers and rotation and deflection gages were recorded after each increment of displacement. When inelastic action was evident in the test specimen, all readings were taken after approximately a ten to fifteen-minute waiting period in order to allow the yielding process to stop and the specimen to come to static equilibrium.

Using the screw jack at the top of the column monotonically increasing lateral joint displacement, $\Delta/2$, was applied to each restrained column until the joint displacement exceeded that corresponding to the stability limit load. This meant that for RC-1, the initial lateral load at the column top decreased at first with increasing lateral displacement and then increased after the stability limit load was reached. For RC-2 and RC-3, the initial lateral load increased at first and then decreased following the stability limit load.

Following the initial test of each specimen as described above, each restrained column was subjected to several cycles of reversed lateral displacement. The results of these cyclic tests will not be reported herein.

5. TEST RESULTS

5.1 Initial Moments

The theoretically calculated loads which were to be applied to each specimen at the start of each test are shown in Fig. 4. However, the loads actually applied corresponding to zero-sway position were slightly different from the theoretical ones in tests RC-1 and RC-3. The loads applied to RC-1 and RC-3 are shown in Figs. 18 and 19, respectively. The numbers in parentheses correspond to the theoretical values. The differences in the horizontal loads resulted from initial imperfection of the columns and the small misalignments during the test setups. In the presence of high axial loads as in these tests, a slight imperfection or misalignment of a column results in a considerable change in the horizontal load. The differences in column axial loads were due to the small variation in oil pressure of the hydraulic jacks of gravity load simulators during the tests.

The bending moment diagrams (plotted on tension sides of members) for three test specimens in the zero sway position are shown in Figs. 20, 21 and 22. In the figures the dotted lines indicate the theoretical moment diagrams determined from the loads actually applied. The solid lines indicate the moment diagrams computed from measured strains. The differences between the theoretical and computed moment diagrams are fairly significant for specimens RC-1 and RC-2. The rather large difference between moment diagrams could arise from:

(1) loads acting through initial imperfections in a specimen,

(2) welding residual moments, (3) elastic shortening of the restrained column under axial loads, and (4) moments due to eccentricities of the column axial load with respect to the column centerline.

The analysis of the experimental data from test RC-1 indicated that there was a restraint coming from the roller guides at the exterior end of the beam. About 30% of the horizontal load in the zero-swayed position was being resisted in the roller guides. Therefore an important source for the large discrepancy between the moment diagrams for specimen RC-1 was the effect of the restraint in the roller guides. The restraint resulted from a small misalignment of the roller guides. In tests RC-2 and RC-3, this restraint was reduced considerably by aligning the roller guides much more carefully.

5.2 Experimental Behavior

The experimental behavior of the three test specimens will be presented and discussed with reference to Figs. 23 to 36 inclusive. Theoretical comparisons and detailed analysis of test results will be discussed in Chapter 6.

In each figure the load points corresponding to applying the initial increments of column axial load P and beam loads are not shown. The indentifying load numbers for each increment of the horizontal joint deflection $\Delta/2$ are given on each experimental curve shown as the solid line in the figures. The theoretical predictions are shown by the dashed curves.

All the plotted points on the curves represent static equilibrium positions of the specimen. After passing the elastic range, the redistribution of strains in the regions loaded above the yield point was

relatively slow. This redistribution of strains resulted in increases in horizontal joint deflections and a decrease in the horizontal jack load from the condition immediately after incrementing the joint deflection. The stabilization of the horizontal load monitored from the load cell at the top of the column was used to indicate when the redistribution of strains had essentially halted and static equilibrium had been attained.

5.2.1 Test Specimen RC-1

The experimental horizontal-load versus sway-deflection curve for test specimen RC-1 is shown in Fig. 23. In the figure, the non-dimensionalized horizontal load, $\frac{Qh}{2M_{pc}}$ and sway deflection, $\frac{\Delta}{h}$ are used, where M_{pc} is the reduced column plastic moment in the presence of axial load and h and Δ are shown in the figure.

In the zero-swayed position, a few yield lines were present in both flanges of the column and distributed throughout the length. This was due to high axial load ratio used ($P/P_y = 0.7$) and the magnitude of residual stresses in the flanges (Fig. 5). However, there was no yielding observed in the beam. As previously shown in Fig. 18, the initial value of Q was -4.96 kips. As the column top deflection was incremented in the direction of Q as shown in Fig. 23, the absolute value of Q initially decreased.

At Load No. 4 in Fig. 23, the top flange of the beam at the two load points started to yield. As the sway deflection increased, yielding was observed in both flanges. At Load No. 6, the web started to yield under the east load point where a plastic hinge was expected to form. At Load No. 8, the web yielding at the east load point had propagated to the center and the web at the west load point started to yield.

At Load No. 11 there were indications of lateral buckling of the beam, and at Load No. 12 definite lateral buckling was observed of the compression flange midway between the west load point and the center of the beam. Following Load No. 12 the horizontal load increased rapidly (in the direction opposite to the joint deflection) as the lateral buckling progressed. The observed lateral buckling was attributed to the movement of a brace near the buckled region, which might have been the result of slippage of the brace. At Load No. 14, the test was concluded and the specimen was then subjected to cyclic loading.

Figure 24 shows the deflected shape of test specimen RC-1 at a number of deflection increments (the numbers on the shapes correspond to the load numbers in Fig. 23). Due to the effects of the extensive yielding of the beam in the region between two load points, a relatively large deflection of the beam was observed. The horizontal deflection of the column top was about twice that of the joint at each stage, as expected.

Figure 25 shows the variation in the axial load ratio of test specimen RC-1. There were no significant changes from the theoretically assumed value of $P/P_y = 0.7$.

The deformed specimen after the completion of cyclic testing is shown in Fig. 26. The severe deformation and yielding on the beam and the column shown in the figure can be partially attributed to the cyclic test. However, similar deformation appeared but to a lesser extent during the test reported herein.

5.2.2 Test Specimen RC-2

The non-dimensionalized horizontal-load versus sway-deflection curve obtained from the test is given in Fig. 27. Because of the symmetry

of the specimen and its vertical loads, there was no initial horizontal force in the zero sway position ($Q = 0$, $\Delta/h = 0$).

As in test RC-1, compression yield lines were observed on the flange tips of the column and were scattered throughout the length in the zero-swayed position. At Load No. 4 severe yielding was observed in the flanges of the west beam adjacent to the column, where the first plastic hinge was expected to form. At Load No. 5 the yielding had progress to the inside face of flanges but there was no apparent yielding on the web. From Load No. 6 the yielding of the west beam near the joint progressed rather slowly as the sway-deflection increased. Up to Load No. 10, there was no pronounced indication of the formation of a plastic hinge in the west beam. At Load No. 11, the yielding had penetrated into the web of the beam. A significant amount of yielding was also observed in the west flange of the column just below the joint. At Load No. 13 the maximum horizontal load of 4.45 kips was attained. On further incrementing the deflection, the horizontal load started to drop rather slowly. At Load No. 16 the test was terminated.

The deflected shape of the beams and column is plotted in Fig. 28. The increase in column deflection was almost linear in the elastic range. However, as the moment at the top of the restrained column approached its reduced plastic moment value and considerable plastification of the column occurred in that region, a slight "kink" developed in the yielded zone and non-linear deflections were then obtained. The column deflection below the joint was then observed to increase with the increasing rate while the rate of deflection of the column above the joint reduced. This behavior is to be expected and is a consequence of the column hinge action.

Figure 29 shows the variation in axial load ratio in the restrained column during the test. The applied axial load ratios were slightly on the high side.

The measured rotations near the joint were plotted for each Load No. in Fig. 30. The locations of the rotation gages are as shown in Fig. 30. The numbers on the plots correspond to the load numbers in Fig. 27. Except for the irregular rotation measured at Location 4, the curves confirm the previously described behavior of the specimen near the joint. Comparing the rotations at Locations 1 and 2, the difference in magnitudes becomes significant as the sway deflection increases, due to the effects of the gradual plastification of the restrained column and the subsequent plastic hinge formation. Similar behavior is also observed in the rotations at Locations 3 and 4.

The specimen after test is shown in Fig. 31. The yielding of the restrained column has been amplified by the cyclic tests. It can be seen that there was little yielding of the beams.

5.2.3 Test Specimen RC-3

The non-dimensionalized horizontal-load versus sway-deflection curve for test specimen RC-3 is shown in Fig. 32. The initial horizontal load at the zero-sway position was 5.52 kips and in the same direction as the imposed sway deflection. As in the previous tests, at zero sway, compression yield lines developed in the flange tips of the column. At Load No. 2, the severe yielding progressed in the west flanges of the restrained column and throughout the length. At Load No. 3, the yielding penetrated into the web of the column, resulting in an extensive yielding of the west half of the restrained column near the connection.

On further loading the frame continued to deflect under the almost constant horizontal load. From Load No. 6 the horizontal load dropped slowly. At Load No. 8, the test was terminated and cyclic loading began.

The deflected shape of specimen RC-3 is shown in Fig. 33. The nature of the column deformation was similar to that of RC-2. The kink near the top of the restraining column was even more distinct in this case. As the sway deflection was increased after the formation of the column plastic hinge, the hinge action was so marked that there was almost no relative increase in deflection between the joint and the top of the column. Nearly all the deformations resulted from the sway increment were concentrated in the plastic hinge region.

The variation in axial load during the test is plotted in Fig. 34. The variation was rather scattered, compared with RC-1 and RC-2. However, the magnitude was not appreciably different from the theoretically assumed value of 0.7.

Figure 35 shows the measured rotations near the connection. The locations of the measuring gages are given in the figure.

The deformed specimen after the test is shown in Fig. 36. The lateral buckling of the beam shown in the figure occurred during the cyclic loading. There was no indication of the lateral buckling during the test reported herein.

6. THEORETICAL COMPARISONS AND DISCUSSION

6.1 Theoretical Prediction

The theoretical horizontal-load versus sway-deflection curves for each of the restrained columns can be generated from restrained column theory[7] and sway subassemblage theory.[1] The theoretical prediction curves for the three restrained columns are shown as the dashed lines in Figs. 23, 27 and 32.

In the theoretical calculations, the column height was taken as the total distance between the pinned ends, which resulted in a strong axis slenderness ratio h/r_x of 34. The clear span of each beam (column face to roller support) was used in all calculations except when calculating the initial (zero-sway) bending moments in the test specimens. In this case, the distance between the column centerline and the roller support was used. Since a beam is able to form a plastic hinge adjacent to the face of a column, the effective length of the beam is assumed to be the clear span length. In calculating the theoretical prediction curves, an axial load ratio of $P/P_y = 0.70$ was used. In addition the measured yield stress levels of the steel were used. For residual stress distribution, the standard residual stress pattern was used.[10]

6.2 Comparative Behavior

6.2.1 Test Specimen RC-1

The difference between the theoretical and experimental values of $\frac{Qh}{2M_{pc}}$ in Fig. 23 in the zero-sway position can likely be attributed to the misalignment of the rollers as discussed in Chapter 5, as well

as the initial out of straightness of the column. The horizontal force exerted by the rollers was observed to be present up to about Load No. 2 which could account for the marked difference in slope between the theoretical and experimental curves in that region. Beyond Load No. 2 it was apparent that the rollers had aligned themselves so that little or no horizontal force was being taken by the rollers. Consequently the slopes of the theoretical and predicted curves in Fig. 23 between Load Nos. 2 and 4 (first yielding) are more nearly the same.

Therefore, the apparent increased stiffness of test specimen RC-1 as shown in Fig. 23 can be attributed mainly to the small friction developed in the roller supports due to the observed initial misalignment. It can be appreciated from observing the small values of horizontal load Q required to cause lateral displacement that very little friction was required to substantially alter the experimental behavior. The small lateral force requirements, of course, are a result of the very high level of axial column load.

Theoretically the lateral load Q for test specimen RC-1 is expected to decrease almost linearly until a plastic hinge forms under the load point nearest the column which results in the failure mechanism for the specimen. As shown in Fig. 23, the lateral load was nearly constant between Load Nos. 6 and 10. The difference between the experimental and theoretical results can be explained by considering the gradual yielding process in the vicinity of the plastic hinge location. Figure 37 shows the experimental variation in the bending moments in test specimen RC-1 at the center of the joint and under the load point closest to the column. In the Figure M_u and M_L are the bending moments at the joint as calculated from the measured strains in the columns

above and below the joint respectively. M_f is the bending moment under the load point as calculated from the measured beam strains. M_B is the bending moment at the joint computed from the measured beam strains. M_B is to be compared with the curve showing $-(M_u + M_L)$.

Although first yielding of the beam was calculated to occur at Load No. 7 (Fig. 37), it occurred as early as Load No. 4 (Fig. 23). This was probably due to welding residual stresses at the load point. It can be observed from Fig. 37 that the gradual plastification of the beam under the load point after first yielding would have the effect of decreasing the lateral stiffness of the test specimen, thus increasing lateral deflection and PΔ effects. As a result, for test specimen RC-1 the applied lateral load for a particular value of lateral deflection would be expected to be greater than predictions based on elastic-plastic beam behavior. Although Fig. 37 indicates that M_p of the beam was not quite reached, some experimental error should be expected as indicated by the difference in calculated joint moments (M_B versus $-(M_u + M_L)$). It was observed during the test that a plastic hinge had developed in the beam under the load point at Load No. 10. As previously discussed in Chapter 5, the beam began to exhibit lateral buckling of the compression flange between the two load points. This was observed to begin after Load No. 10, with definite lateral buckling at Load Nos. 11 and 12.

Figure 38 shows the strain distribution in the beam flanges at the strain gage location nearest the center of the laterally buckled region. The numbers in the figure correspond to the load numbers in Fig. 23. It can be seen that the first indication of lateral buckling was at Load No. 11 and there was a definite lateral buckling at Load

No. 12. Since the strain gage location was about 14 in. away from the center of the laterally buckled region, the strains shown in Fig. 38 will be somewhat smaller than the maximum strains in the beam due to lateral buckling. From Figs. 37 and 38 it is evident that in the vicinity of Load Nos. 10 and 11 a plastic hinge had almost developed in the beam under the load point nearest the column, which is in fairly good agreement with observed behavior. In addition lateral buckling of the beam was well developed, at least after Load No. 11. As a result, additional beam restraint was no longer available to the restrained column following Load Nos. 10 and 11. The subsequent unloading of the restrained column could therefore be expected and is confirmed by Fig. 23. Since no strain-hardening occurred in the beam following unloading (except that associated with lateral buckling), the unloading slope of the restrained column curve could be expected to agree closely with theoretical predictions as shown in Fig. 23.

In conclusion, considering the difficulties with the initial alignment of the rollers and the initial lateral friction force which was developed at the start of the test of specimen RC-1, the experimental and theoretical behaviors of this restrained column are in fairly good agreement.

6.2.2 Test Specimen RC-2

Figure 27 shows the experimental load-deflection curve and the theoretically predicted curves for test specimen RC-2. In the theoretical calculations, two different analysis were made. In analysis 1, the beam plastic hinge is assumed to form at the face of the column. In analysis 2, the beam plastic hinge is assumed to form away from the column face, at a distance equal to the beam depth.[11,12]

The prediction based on analysis 1 indicated that the first plastic hinge forms in the beam (Fig. 4). The second plastic hinge occurs at the top of the restrained column following an instability failure of the restrained column at a lateral load of 4.25 kips ($\frac{Qh}{2M_{pc}} = 0.58$). The theoretical prediction based on analysis 2 indicates that the first and only plastic hinge occurs at the top of the restrained column at a maximum lateral load of 4.60 kips ($\frac{Qh}{2M_{pc}} = 0.63$).

As shown in Fig. 27, the initial behavior of test specimen RC-2 was almost linear and followed very closely the predicted curves. Theoretically, the load-deflection curve should start at the origin ($\frac{Qh}{2M_{pc}} = 0$, $\frac{\Delta}{h} = 0$). However, there was a small initial deflection with zero lateral load at the start of the test. This can be attributed to the errors occurred during alignment.

As previously stated, according to analysis 1, the first plastic hinge should form in the beam at the column face with a horizontal joint deflection of about 0.33 in. In the test, at Load No. 8 where nearly the same deflection was attained, the moment in the beam at the column face was considerably below the plastic moment. This moment is plotted in Fig. 39 as M_c. In Fig. 39, moments M_c, M_D and M_L were calculated from measured strains in the beam and the column as described before. At Load No. 11 the moment M_c exceeded the theoretical plastic moment capacity which was in good agreement with visual observation, since it was observed that yielding had penetrated the web of the beam near the column face. After reaching the theoretical plastic moment, the moment at the column face was continued to increase, but at a smaller rate. This increase can be attributed to the effects of the

constraint from the connection and the strain-hardening at the yielded region. It is apparent from Fig. 39 that a plastic hinge at the top of the restrained column was obtained at Load No. 14. This was also observed during the test. This resulted in the attainment of the collapse mechanism assumed in analysis 1. The experimental behavior as shown in Fig. 27 is in fairly good agreement with the predicted results based on analysis 1.

Theoretically, the horizontal deflection of the column is assumed to increase linearly along the column length. In the test, this behavior was observed in the elastic range. However, as yielding of the restrained column progressed and localized curvature change of the yielded zone occurred, the increase in column deflection became, non-linear and a kink developed in the yielded region just below the joint. The kink became more distinctive with the formation of the column plastic hinge. As a result, the relative change in deflection along the upper column was considerably smaller than that of the restrained column. The $P\Delta$ moment coming from the upper column became less than the theoretically assumed value. This difference in $P\Delta$ moment could be a source of the discrepancy between the predicted and the experimental curves near the instability limit load and in the subsequent unloading curves, where the experimental curve remain higher than the predicted curve as shown in Fig. 27.

During the unloading part of the test, the specimen exhibited somewhat greater stiffness than predicted. This could be attributed to the following sources: (1) the effect of joint stiffness; (2) the effect of strain-hardening; and (3) the smaller $P\Delta$ moment coming from the upper column than that theoretically assumed. The influence of

these effects which result in conservative behavior can be observed from the following analysis of the test data, where an attempt was made to eliminate strain-hardening from the test results. For Load Nos. 14, 15 and 16, the lateral loads Q corresponding to the measured column moments above M_{pc} were computed and subtracted from the experimentally obtained values of Q. The results are shown in Fig. 40 by the solid circles. The modified test curve is compared with two theoretical curves based on analysis 1, using two different column slenderness ratios; one with the distance between pinned ends as the column length and the other with the distance between pinned ends less the length of the connection. The experimental results closely agree with analysis 1, assuming that the total column length is the distance between pinned ends. A similar result was found by C. K. Yu and reported in Ref. 13.

6.2.3 Test Specimen RC-3

Figure 32 shows the experimental load-deflection curve and the theoretically predicted curves for test specimen RC-3. The small difference between the theoretical and experimental values of $\frac{Qh}{2M_{pc}}$ in the zero-swayed position can be attributed to a small misalignment during the test setup and out of straightness of the members. At zero-sway the theoretical lateral load at the column top is 5.68 kips ($\frac{Qh}{2M_{pc}} = 0.78$) while the load applied in the test was 5.52 kips ($\frac{Qh}{2M_{pc}} = 0.75$) as shown in Fig. 19.

In the theoretical analysis, the first plastic hinge occurs at the top of the restrained column, which results in the failure of the specimen. In the test, M_{pc} was reached at the top of the restrained column between Load Nos. 3 and 4 as shown in Fig. 41, where the experimental variation of joint moments in the test specimen is plotted.

However, the moment at the joint continued to increase up to Load No. 7 while an almost constant value of horizontal load was maintained as the sway deflection increased (Fig. 32). As discussed in Section 6.2, this behavior probably resulted from the effects of the joint stiffness, strain-hardening and the smaller PΔ moment contributed by the upper column due to the hinge action.

In test specimen RC-3, the hinge action on the horizontal deflection of the column was more distinctive than in test specimen RC-2. The deflection at the column top was much smaller than predicted after the reduced plastic moment in the restrained column was reached. This was an important factor contributing to the significant increased stiffness of the specimen beyond the theoretical mechanism.

In order to evaluate the effects of strain-hardening, the same analysis as in the test specimen RC-2 was performed on the experimental results. Figure 42 shows the modified experimental results as the solid circles where strain-hardening has been eliminated from the test results. The modified test curve is in very good agreement with the theoretical unloading curve. In the figure, the experimental curve is also compared with the theoretical curve determined with the column slenderness of $\frac{h}{r_x} = 30.4$. As in the test specimen RC-2, the experimental result closely agree with the theoretical curve with the total column length between pinned ends ($\frac{h}{r_x} = 34.0$).[13]

Although there is a small difference between the theoretical and experimental curves at the start of the test, two curves are in fairly good agreement during the initial loading part of the load-deflection curve. The maximum horizontal load attained during the test

was 6.06 kips ($\frac{Qh}{2M_{pc}}$ = 0.83) which gives a good agreement with the predicted value of 6.00 kips ($\frac{Qh}{2M_{pc}}$ = 0.82). Since the conservative effects, such as joint stiffness, strain-hardening and reduced PΔ effect, are not considered in the theoretical prediction, there was a considerable discrepancy between the experimental and predicted unloading curves. However, the test of specimen RC-3 was in good agreement with prediction based on restrained column and sway subassemblage theory.

7. SUMMARY AND CONCLUSIONS

Tests were conducted on three restrained columns permitted to sway. Each test specimen represented a restrained column in either a windward, an interior, or a leeward sway subassemblage. The main purpose of the tests was to study the load-deflection behavior of such restrained columns and to compare the experimental results with the predictions from restrained column and sway subassemblage theory. The most important observations are summarized below:

1. The behavior and the strength of all test specimens were in fairly good agreement with the theoretical predictions. The order and location of plastic hinge formation were the same as predicted.

2. As yielding of restrained column progressed, a kink developed in the yielded region and the $P\Delta$ moment contributed by the upper column at the joint became considerably less than the theoretically assumed value.

3. The beam moment at the column face exceeded the full plastic moment capacity of the section, M_p, in a test. However, the experimental result closely agree with the prediction assuming that the beam plastic hinge forms at the face of the column.

4. Due to the effects of the joint stiffness and strain-hardening, the moment at the top of a restrained column exceeded its reduced plastic moment capacity, M_{pc}, when a column plastic

hinge was expected to form. Consequently, the specimens were stiffer than the prediction in the unloading part of the tests. The behavior modified by eliminating the effects of strain-hardening from the experimental results is in very good agreement with the theoretical behavior.

5. Although there is an effect of joint stiffness, the experimental results closely agree with predictions, assuming that the total column length is the distance between pinned ends.

The following conclusions are based on the test results of this investigation:

1. The behavior and the strength of restrained columns permitted to sway with a constant or a variable rotational stiffness can be closely predicted by restrained column and sway subassemblage theory.

2. In the theoretical calculations, the total height of a column and the clear span of a beam should be used, except when calculating the initial (zero-sway) bending moment. In this case, the center-to-center span of a beam should be used.

8. ACKNOWLEDGMENTS

The work reported herein was performed at the Fritz Engineering Laboratory, Department of Civil Engineering, Lehigh University. Dr. David A. VanHorn is the Chairman of the Civil Engineering Department and Dr. Lynn S. Beedle is Director of the Fritz Engineering Laboratory. The results presented form part of a general investigation in "Strength of Beam-and-Column Subassemblages in Unbraced Multi-Story Frames." Sponsorship of the program was provided by the American Iron and Steel Institute. Technical guidance was provided by the Task Force (I. M. Viest, Chairman) on AISI Project 150.

The authors gratefully acknowledge the assistance of Dr. L. W. Lu, Director of the Plastic Analysis Division and Messrs. H. Yoshida and L. D. Carpenter, who gave unvaluable suggestions in planning the tests and their help during testing. The work of Kenneth R. Harpel and the technicians in setting up the tests is gratefully appreciated. Thanks are due also to Miss Karen Philbin who typed the report and Mr. John Gera who prepared the drawings.

9. NOMENCLATURE

A	area of cross section;
b	flange width;
d	depth;
H	horizontal wind load;
h	story height;
I_x	moment of inertia about major axis;
k	restraint stiffness;
M	bending moment;
M_B	bending moment at joint computed from measured beam strains;
M_C	bending moment on beam at column face;
M_D	bending moment on beam at a depth of beam away from column face;
M_f	bending moment on beam under load point;
M_L	bending moment at joint computed from measured strain of upper column;
M_p	plastic moment capacity of cross section;
M_{pc}	reduced plastic moment capacity considering axial load;
M_u	bending moment at joint computed from measured strains of restrained column;
n	level;
P	axial force in column;
P_y	axial yield load of cross section;
Q	horizontal force;
r_x	radius of gyration about major axis;
t	flange thickness;

w	web thickness;
Z_x	plastic section modulus about major axis;
Δ	relative lateral deflection of two consecutive stories;
$\Delta/2$	joint deflection;
δ	axial deformation;
ϵ_y	yield strain;
λ	distribution factor of shear;
σ_y	static yield stress level.

10. TABLES AND FIGURES

TABLE 1 CHEMICAL COMPOSITION AND MILL TESTS RESULTS

Section	Chemical Composition(%)				Mechanical Property		
	C	Mn	P	S	Yield Point (ksi)	Tensile Strength (ksi)	Elongation(8 in) (%)
12B22	0.18	0.63	0.010	0.036	47.3	67.5	29.5
8W40	0.20	0.56	0.014	0.034	51.0	68.4	22.9

TABLE 2 SUMMARY OF TENSION TESTS

		Static Yield Stress (ksi)	Ultimate Stress (ksi)	Elongation (8 in) (%)
12B22	Web	38.5	62.7	29.0
	Flange	33.6	59.5	30.3
8W40	Web	33.3	61.0	30.2
	Flange	32.2	60.7	31.0

TABLE 3 AVERAGE SECTION PROPERTIES

Section		d (in)	b (in)	t (in)	w (in)	A (in^2)	I_x (in^4)	Z_x (in^3)	M_p (kip-in)	P_y (kips)
12B22	Handbook	12.31	4.03	0.424	0.260	6.47	155.7	29.4	1060*	---
	Measured	12.35	4.04	0.412	0.266	6.41	153.1	28.8	1020	---
8W40	Handbook	8.25	8.08	0.558	0.365	11.76	146.3	39.9	1435*	423*
	Measured	8.28	8.09	0.536	0.366	11.32	141.8	38.4	1240	367

*Yield stress taken as 36 ksi

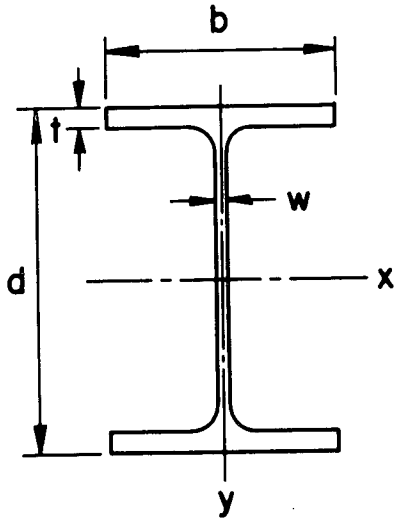

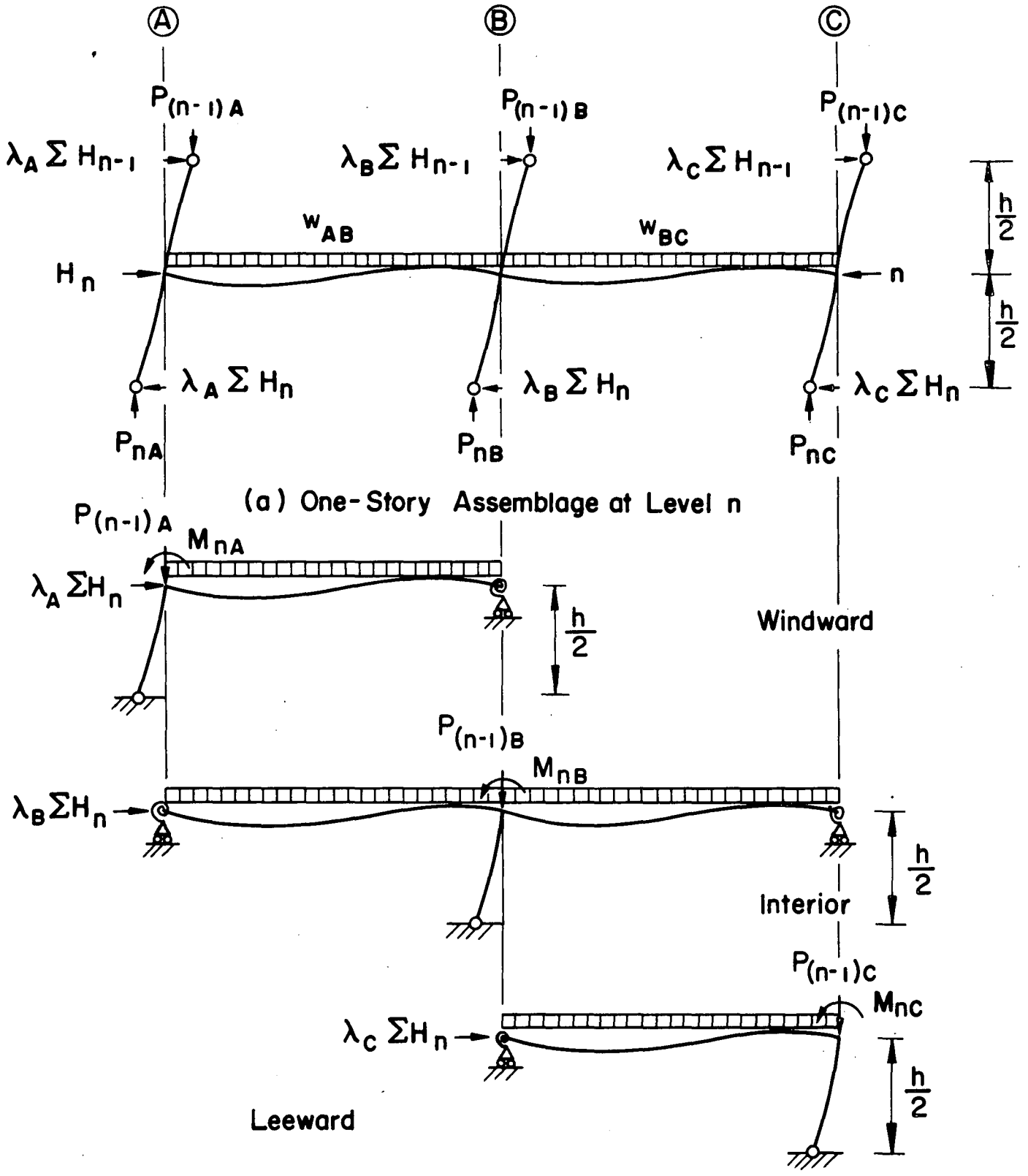

FIG. 1 ONE-STORY ASSEMBLAGE AND SWAY SUBASSEMBLAGES AT LEVEL n

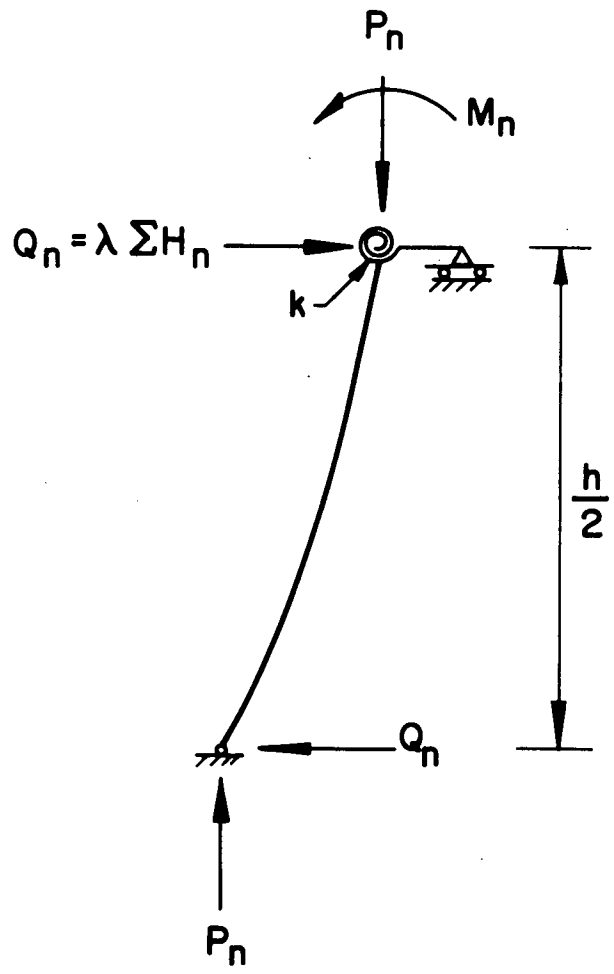

FIG. 2 RESTRAINED COLUMN PERMITTED TO SWAY

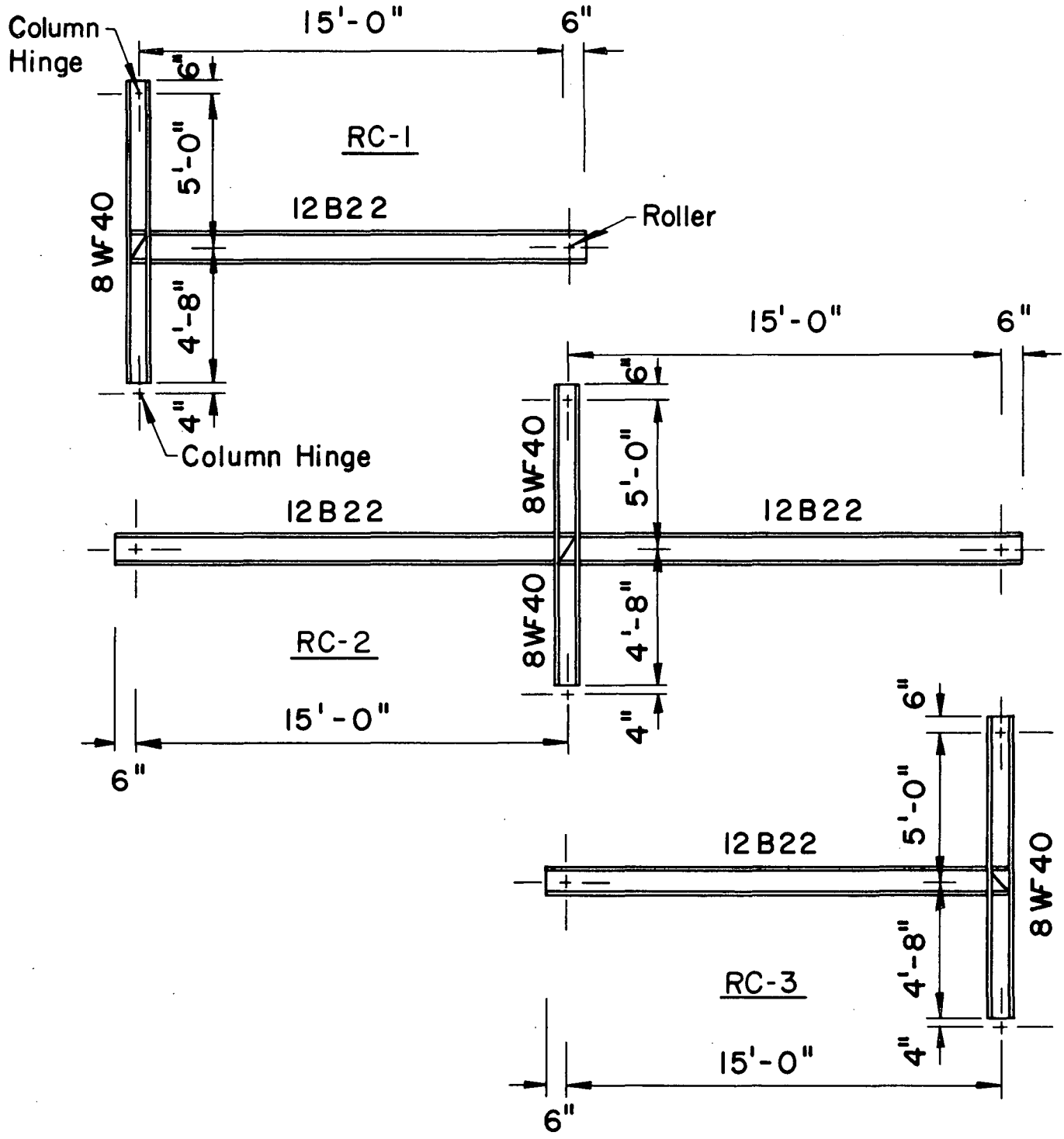

$h = 10"$

$h/r_x = 34$ For All Columns

FIG. 3 TEST SPECIMEN DETAILS

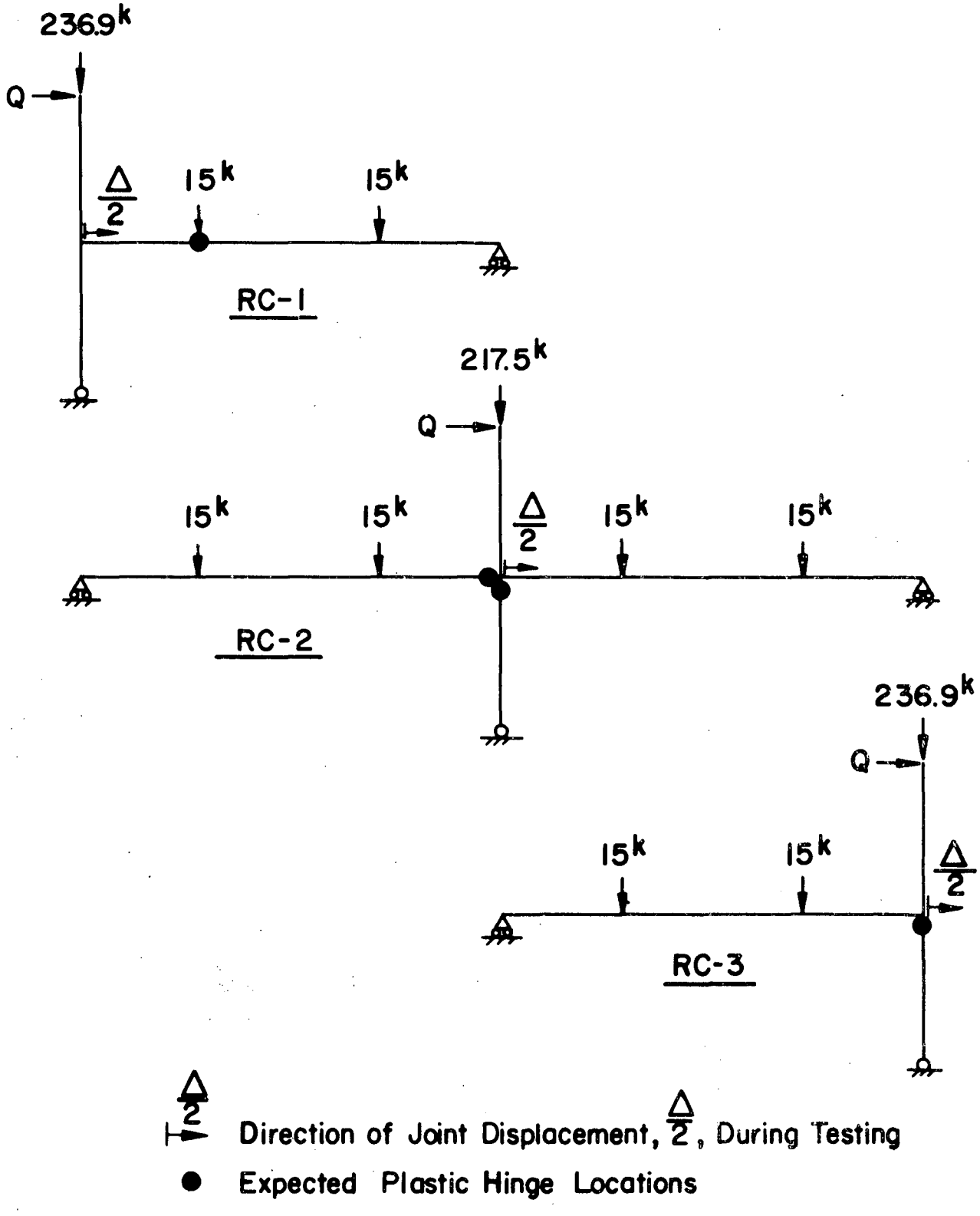

FIG. 4 LOADING AND EXPECTED PLASTIC HINGE LOCATIONS FOR EACH TEST SPECIMEN

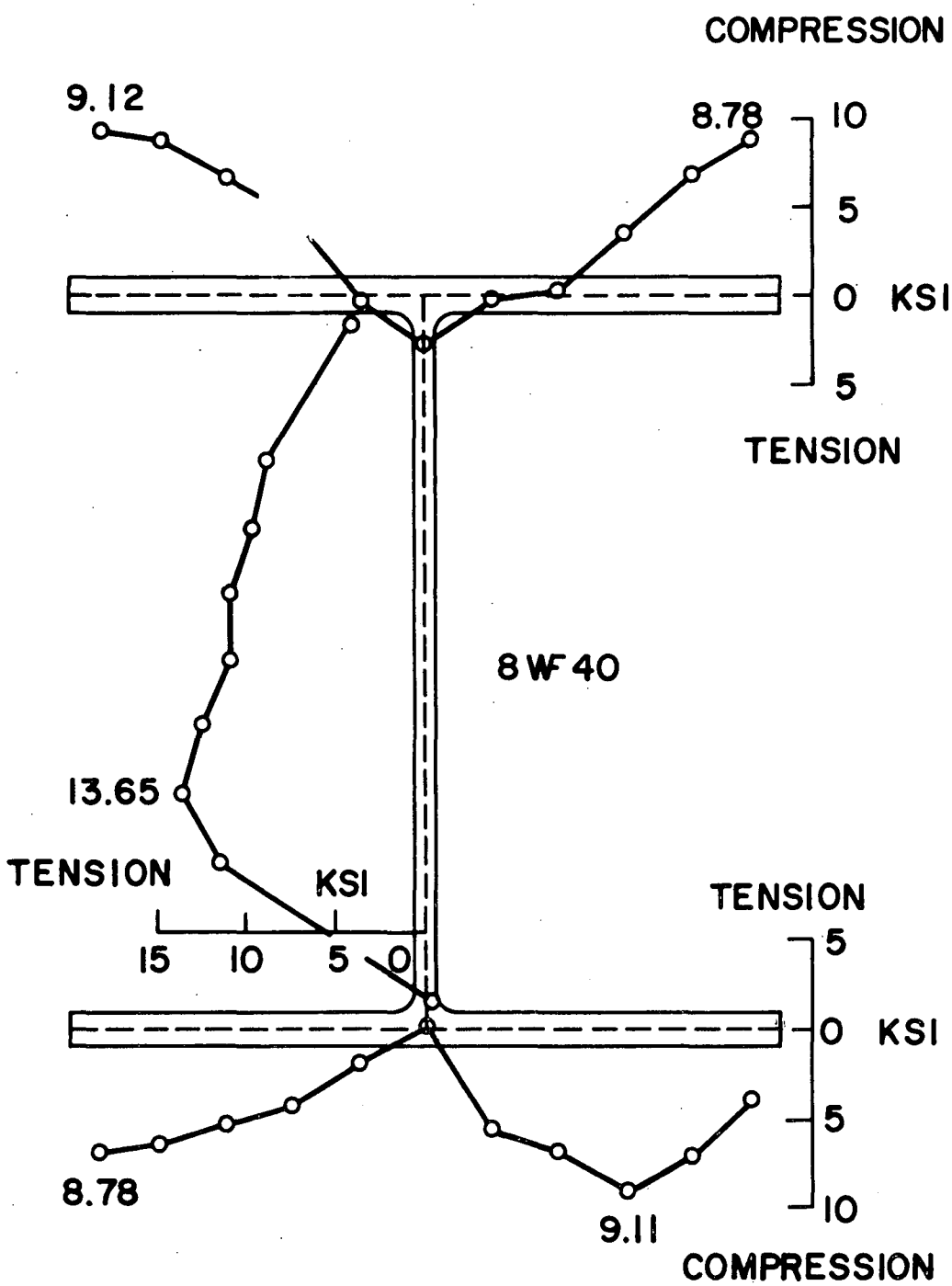

FIG. 5 RESIDUAL STRESS DISTRIBUTION

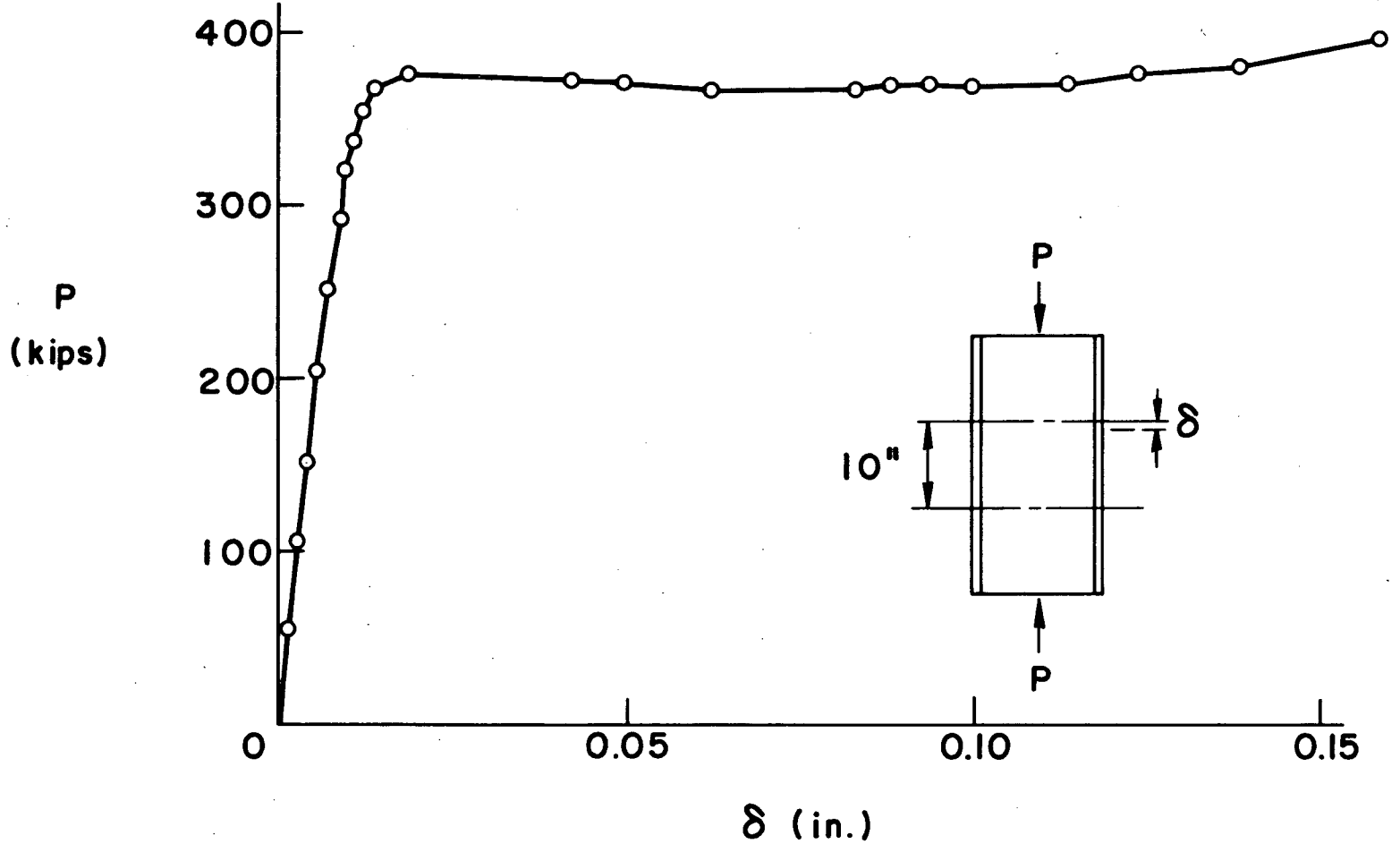

FIG. 6 LOAD DEFORMATION CURVE FROM STUB COLUMN TEST

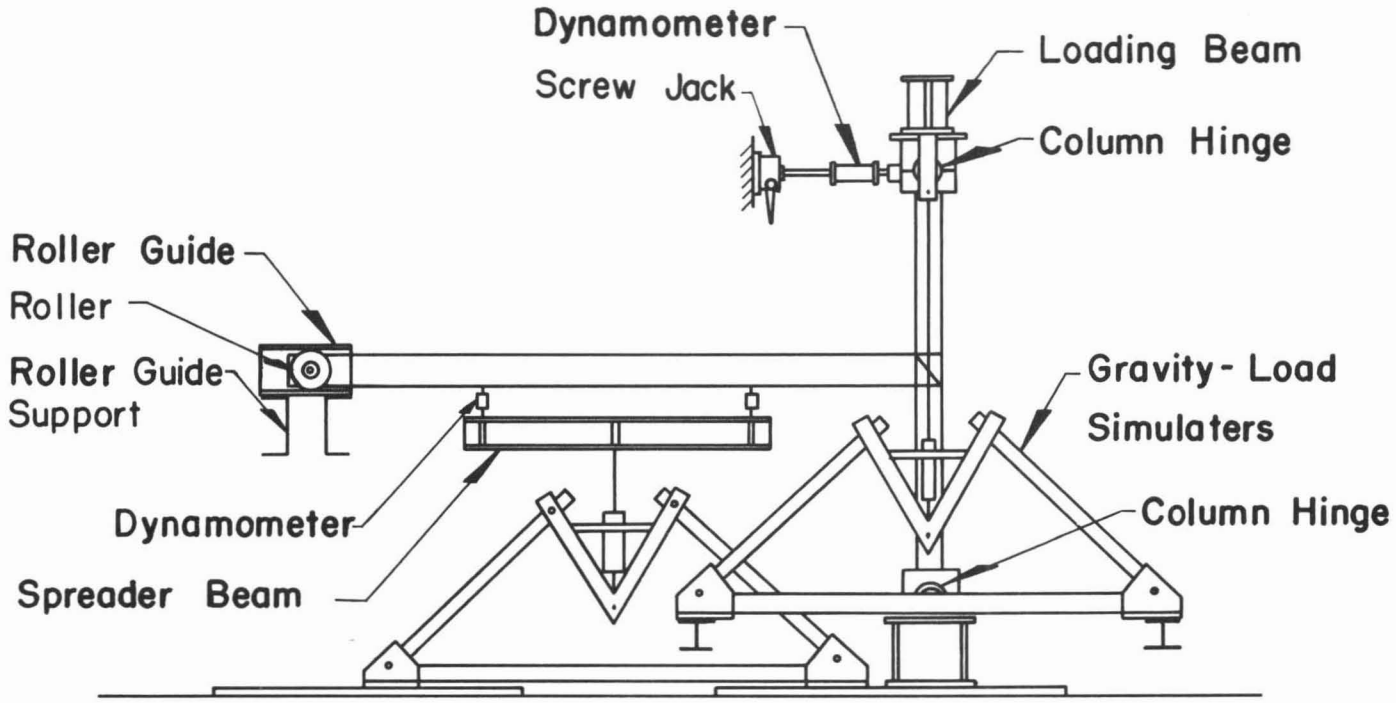

FIG. 7 SCHEMATIC SKETCH OF TEST SETUP FOR TEST SPECIMENS RC-1 AND RC-3

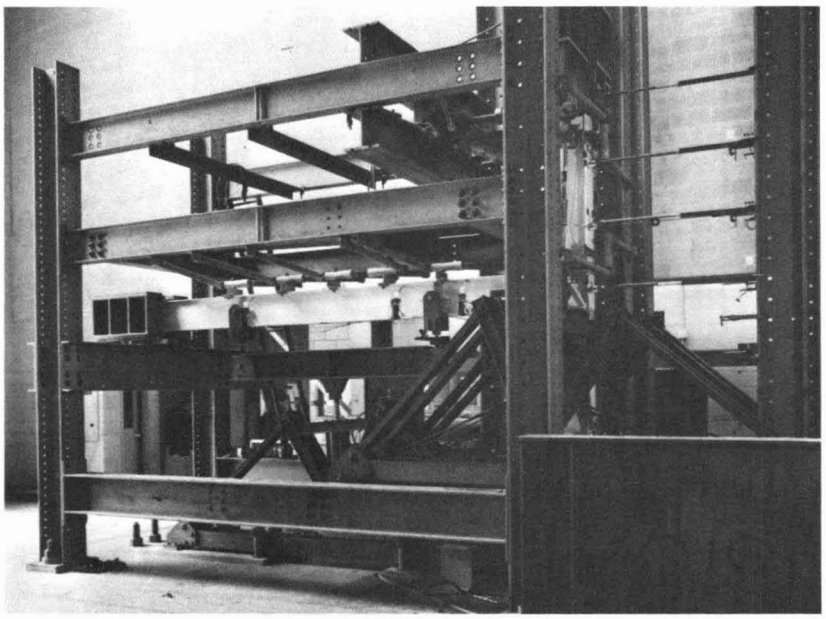

FIG. 8 OVERALL VIEW OF TEST SETUP FOR TEST SPECIMENS RC-1 AND RC-3

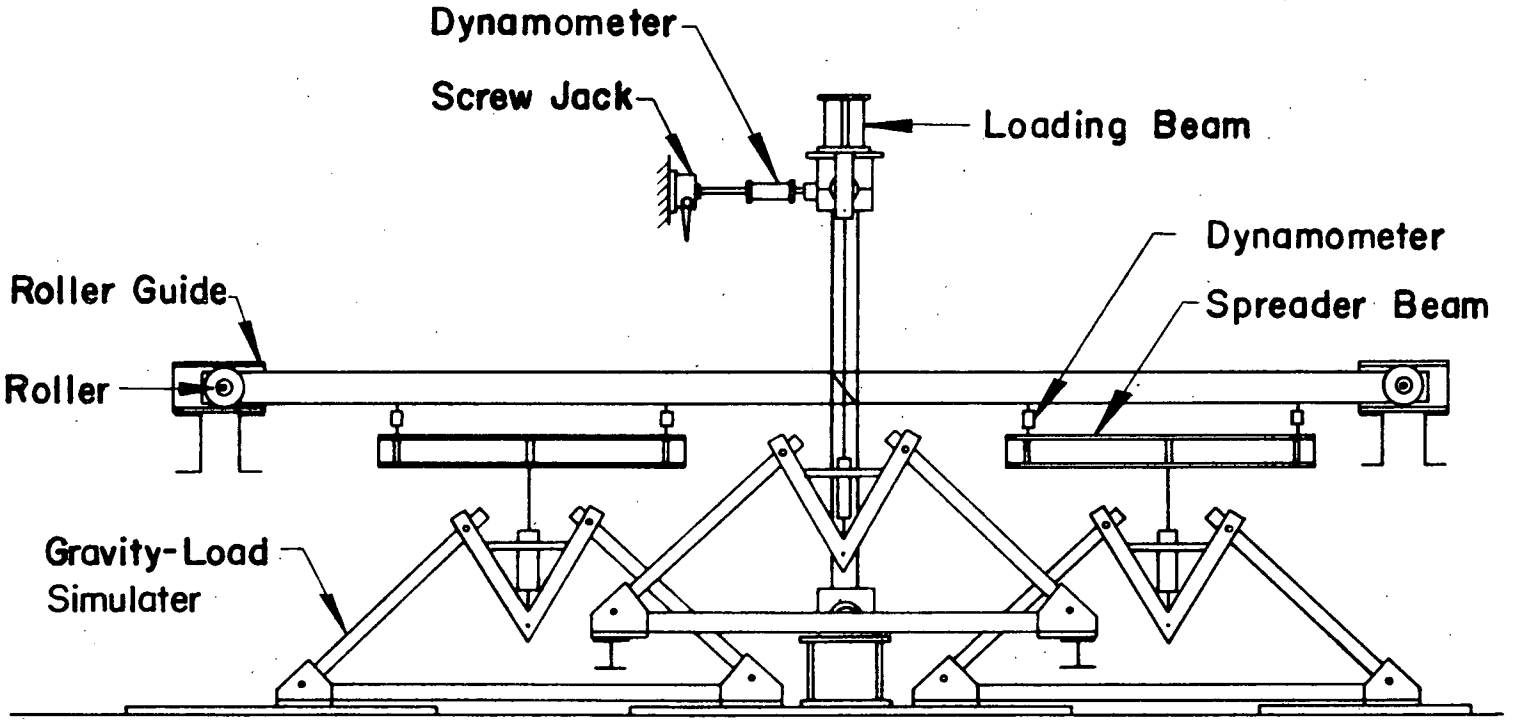

FIG. 9 SCHEMATIC SKETCH OF TEST SETUP FOR TEST SPECIMEN RC-2

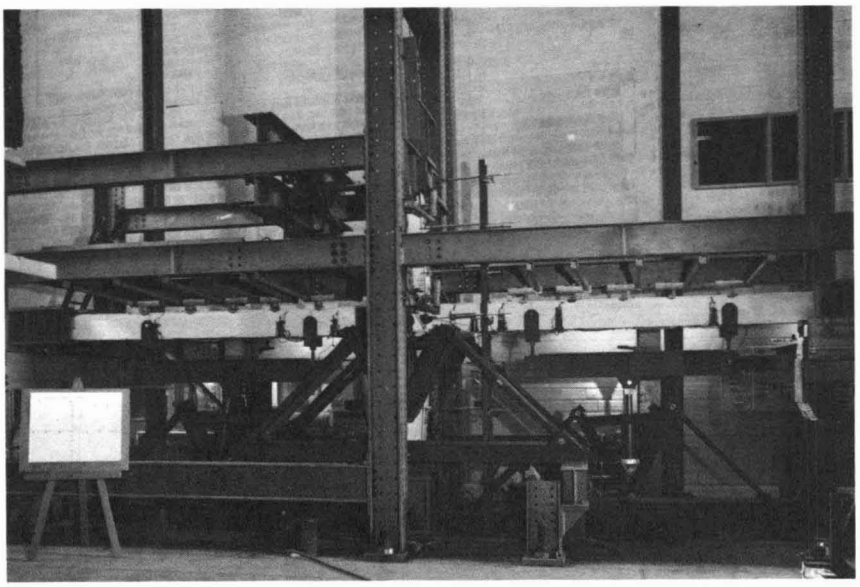

FIG. 10 OVERALL VIEW OF TEST SETUP FOR TEST SPECIMEN RC-2

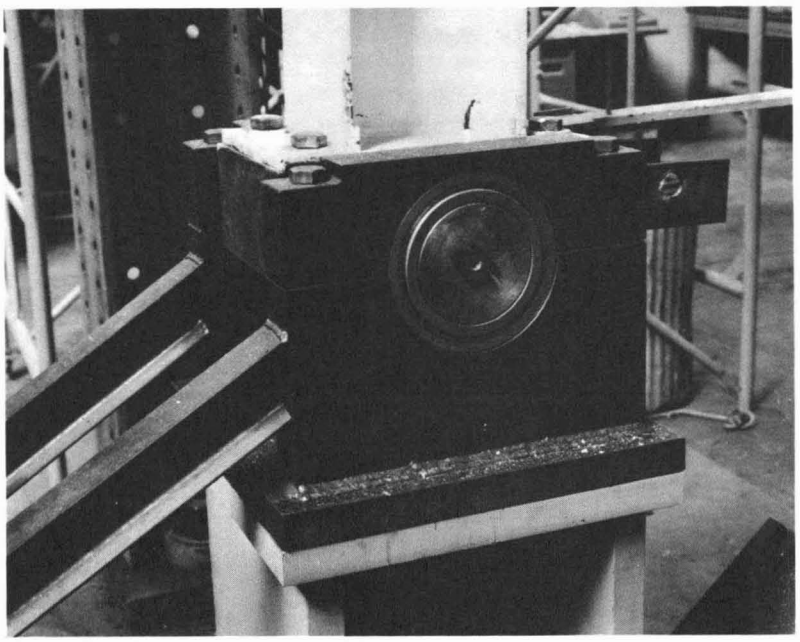

FIG. 11 COLUMN HINGE AND HINGE SUPPORT DETAIL

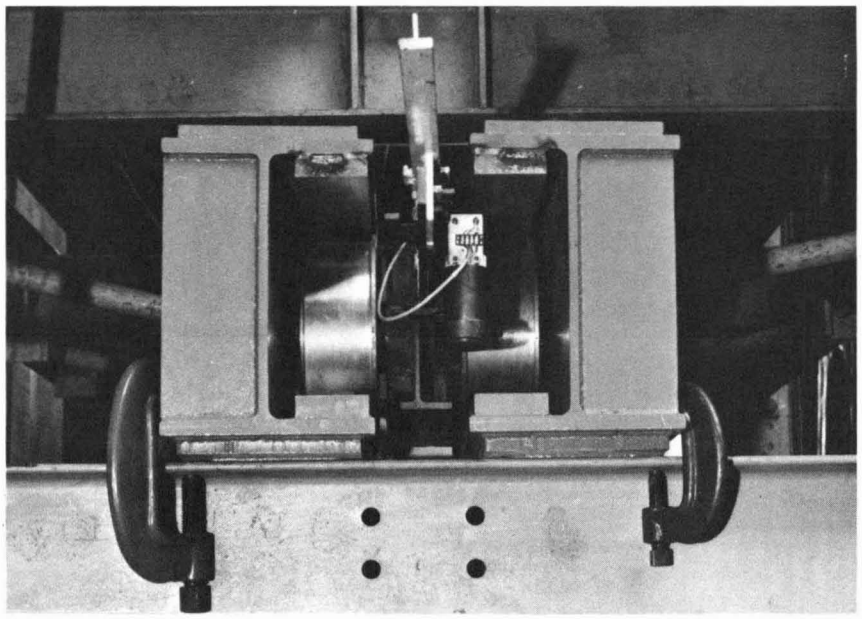

FIG. 12 ROLLERS AND ROLLER GUIDES AT EXTERIOR END OF BEAM

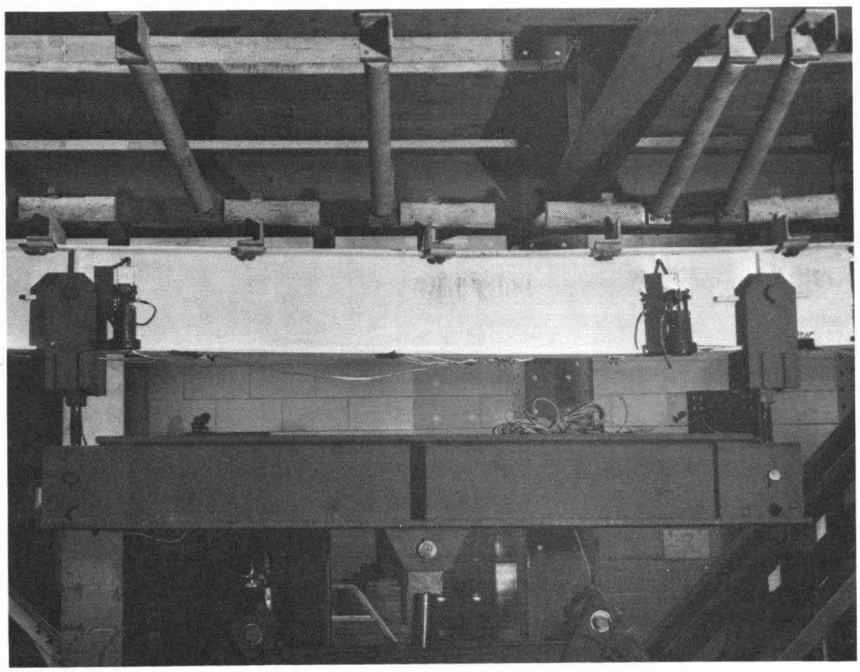

FIG. 13 LATERAL BRACING SYSTEM FOR THE RESTRAINING BEAMS

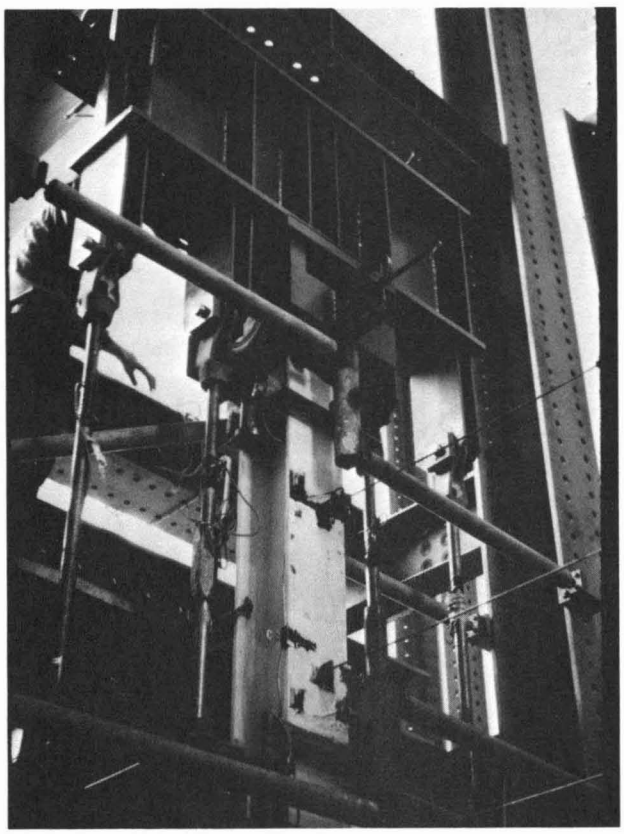

FIG. 14 LOADING BEAM USED TO APPLY VERTICAL LOAD TO COLUMN TOP

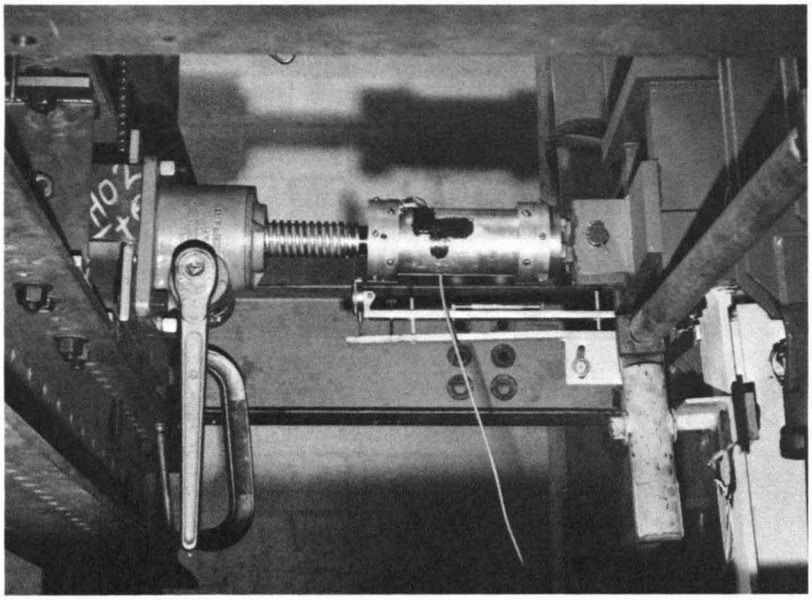

FIG. 15 HORIZONTAL SCREW JACK USED TO DISPLACE COLUMN TOPS

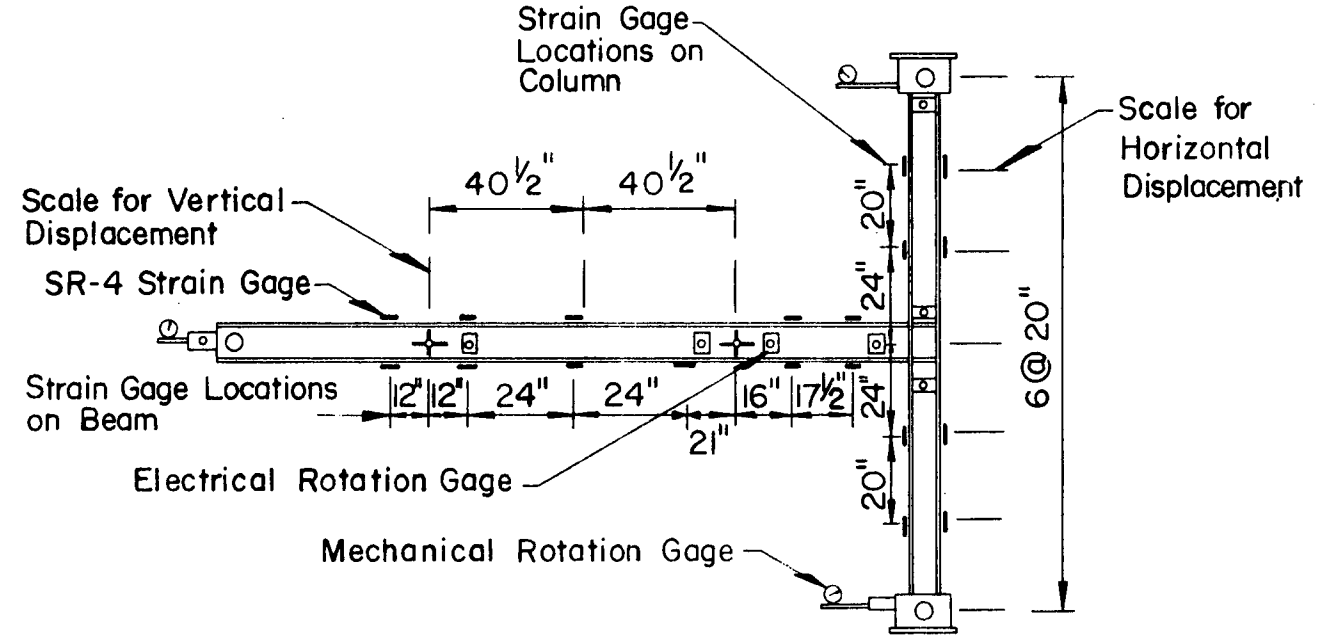

(a) RC-1 and RC-3

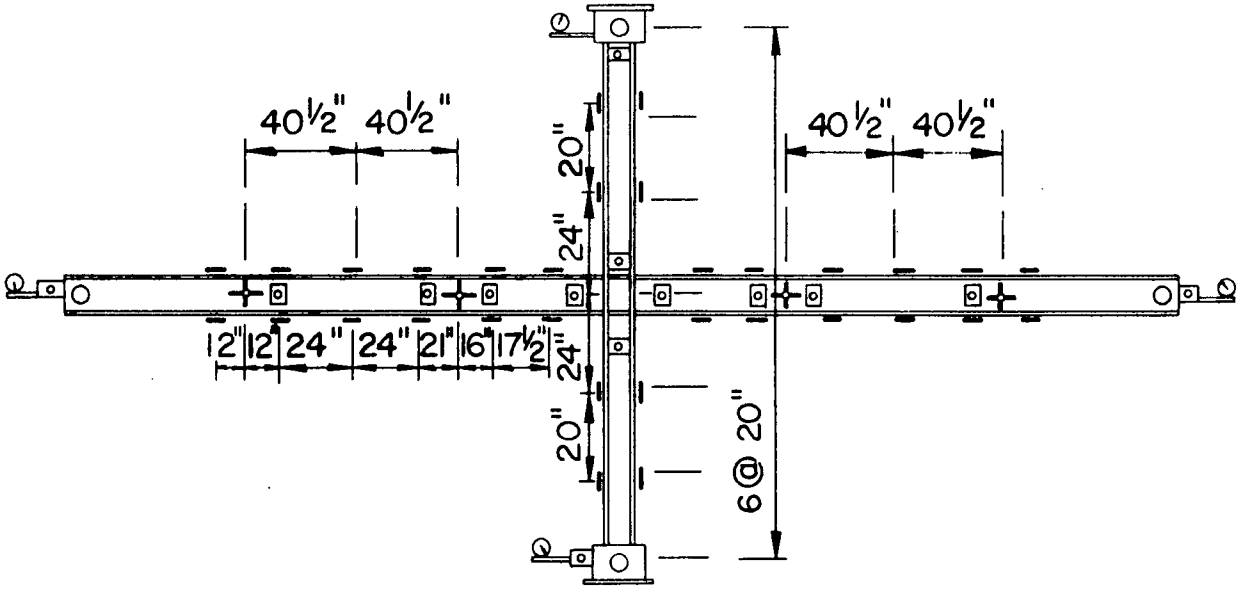

(b) RC-2

FIG. 16 LOCATION OF ELECTRICAL STRAIN GAGES FOR EACH TEST SPECIMEN

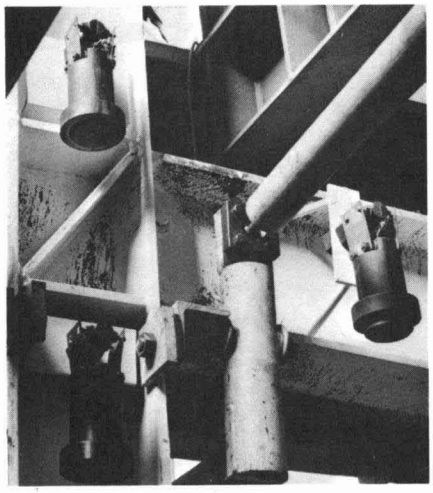

(a) Electrical Rotation Gage

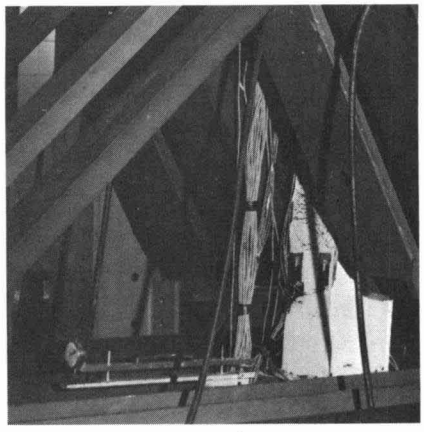

(b) Mechanical Rotation Gage

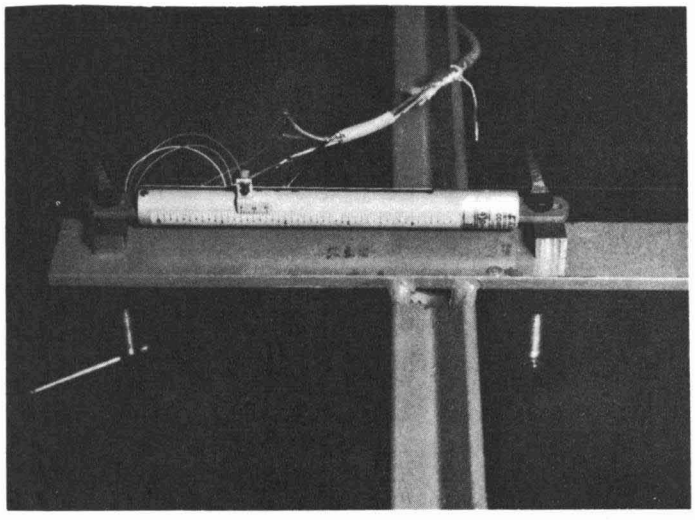

(c) Electrical Displacement Gage

FIG. 17 ROTATION AND DEFLECTION MEASURING DEVICES

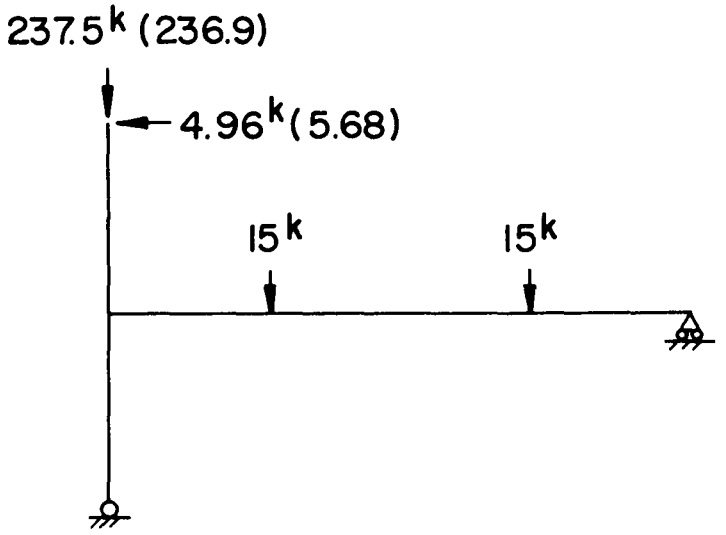

FIG. 18 LOADS ON TEST SPECIMEN RC-1
AT ZERO-SWAYED POSITION

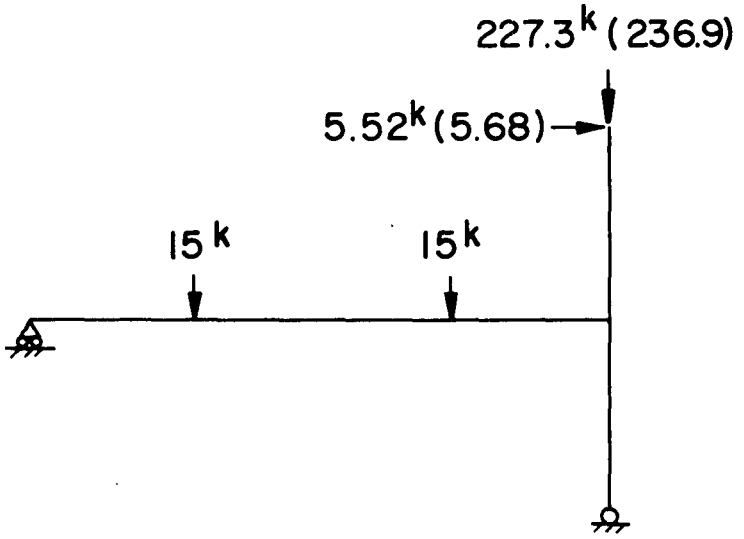

FIG. 19 LOADS ON TEST SPECIMEN RC-3
AT ZERO-SWAYED POSITION

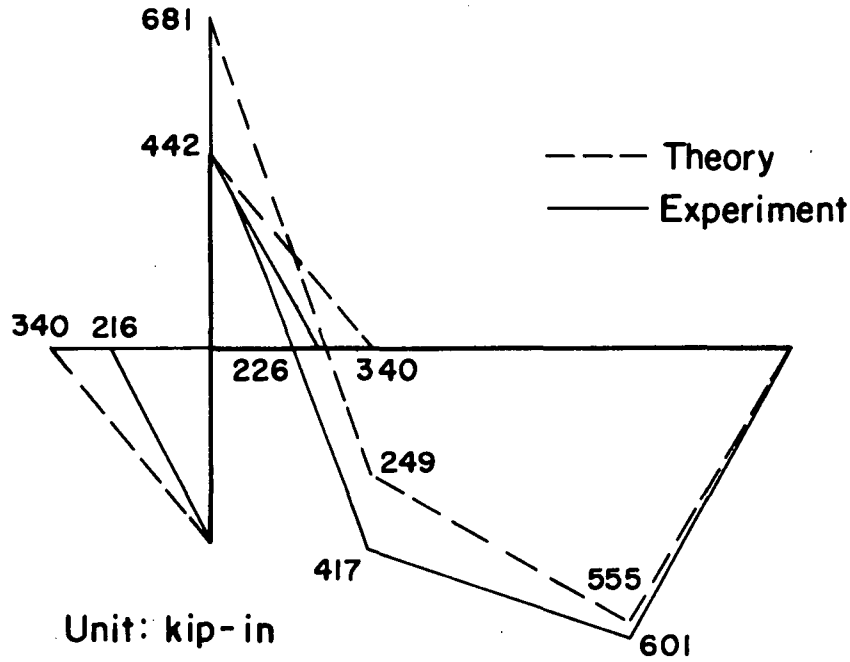

FIG. 20 MOMENT DIAGRAM FOR TEST SPECIMEN RC-1 AT ZERO-SWAYED POSITION

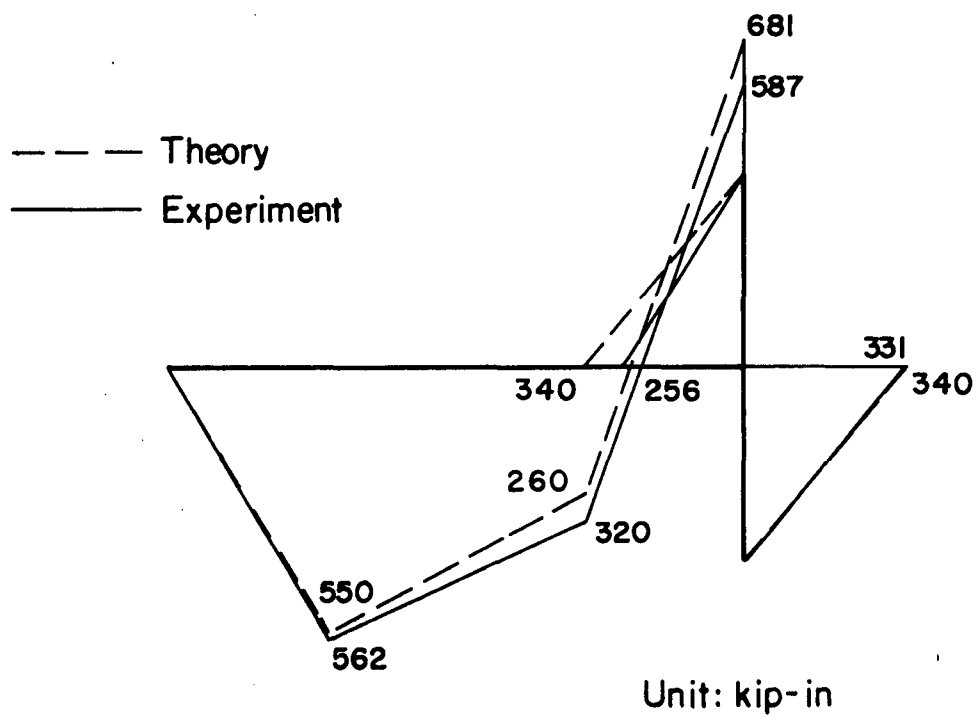

FIG. 21 MOMENT DIAGRAM FOR TEST SPECIMEN RC-3 AT ZERO-SWAYED POSITION

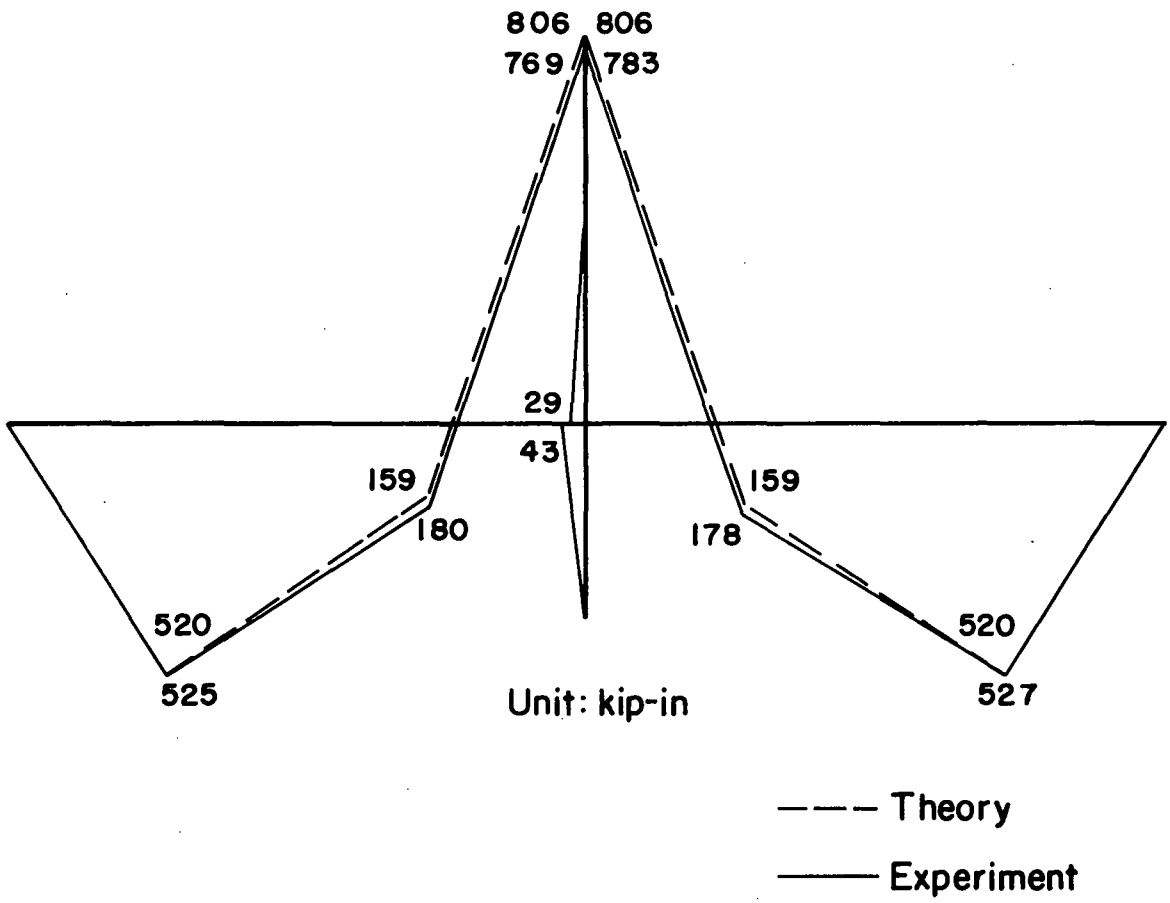

FIG. 22 MOMENT DIAGRAM FOR TEST SPECIMEN RC-2
AT ZERO-SWAYED POSITION

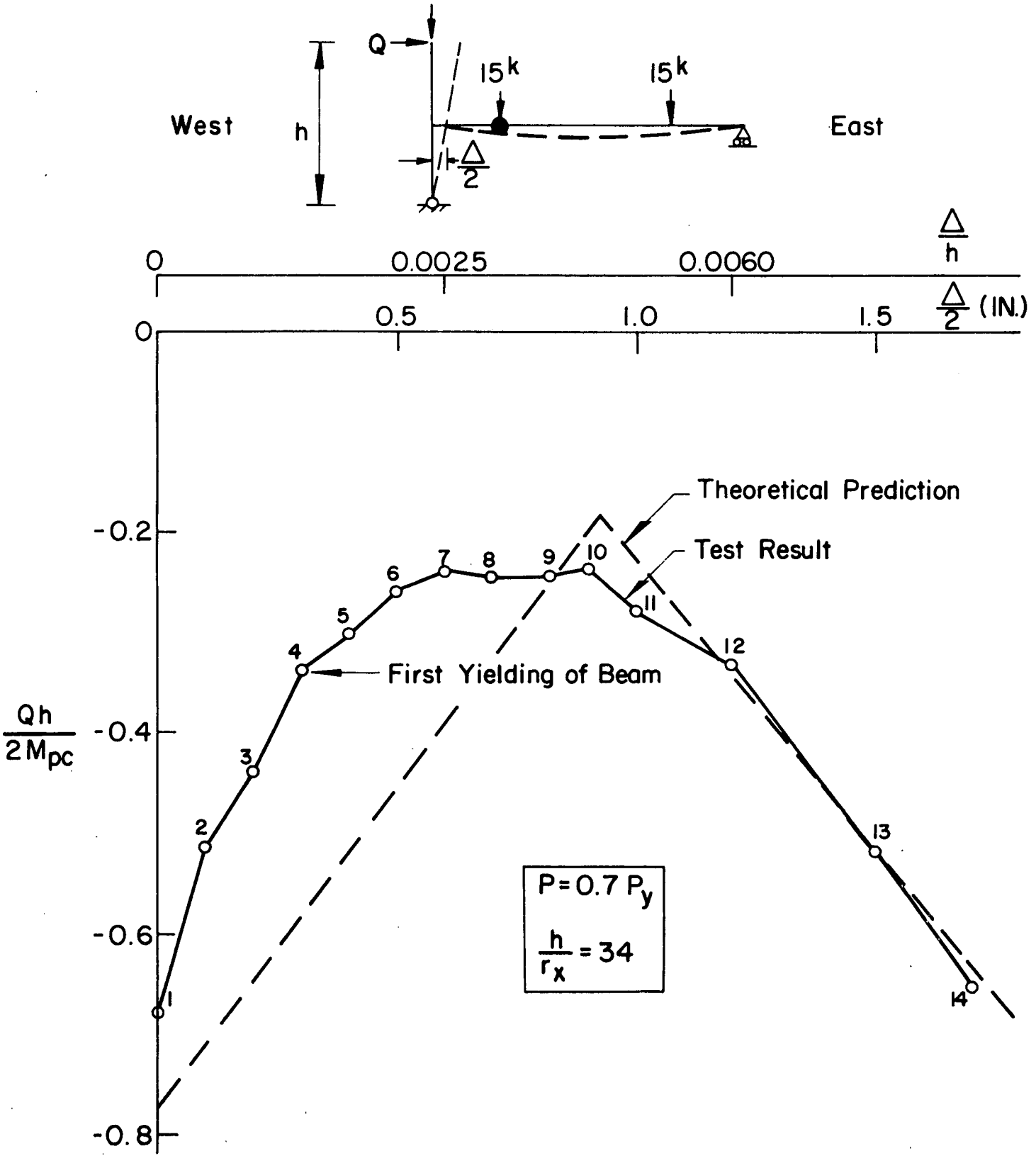

FIG. 23 LOAD DEFLECTION CURVE FOR TEST SPECIMEN RC-1

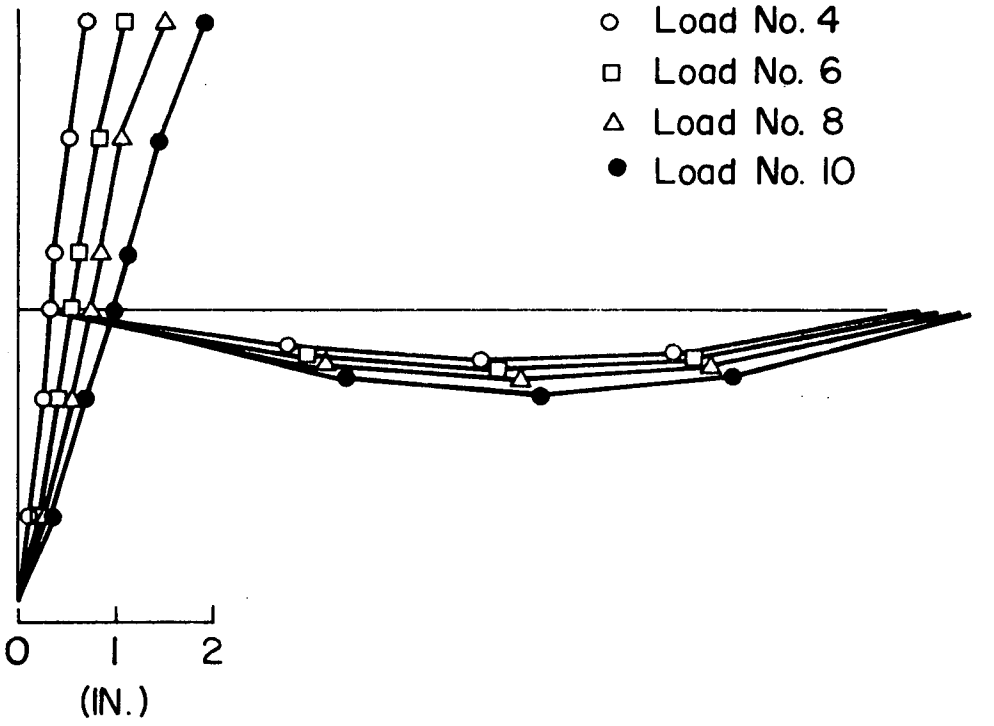

FIG. 24 DEFLECTIONS OF TEST SPECIMEN RC-1

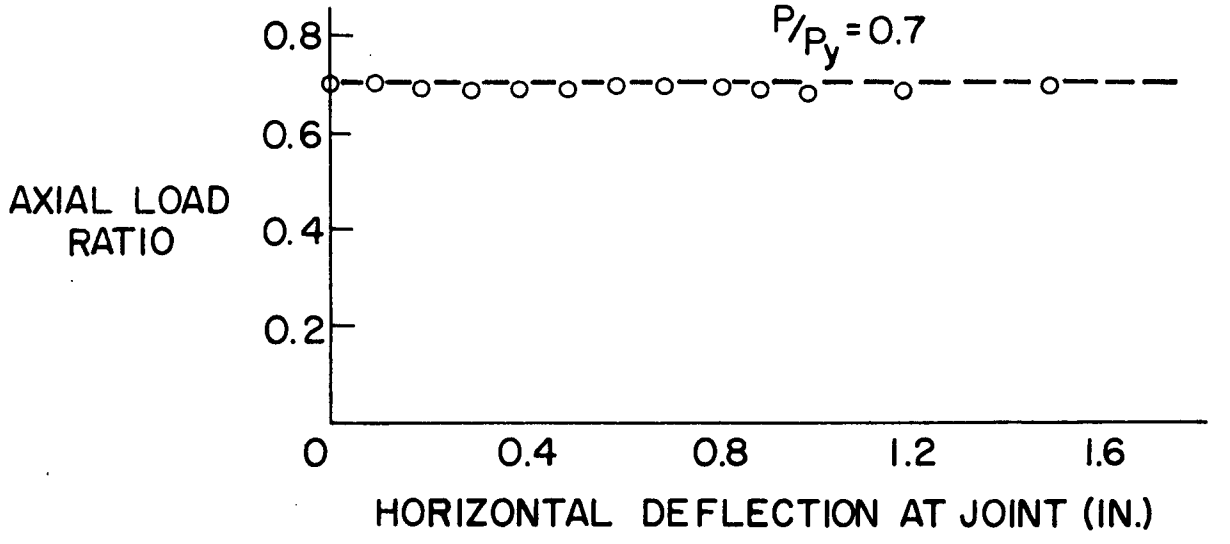

FIG. 25 VARIATION IN AXIAL LOAD RATIO IN TEST SPECIMEN RC-1

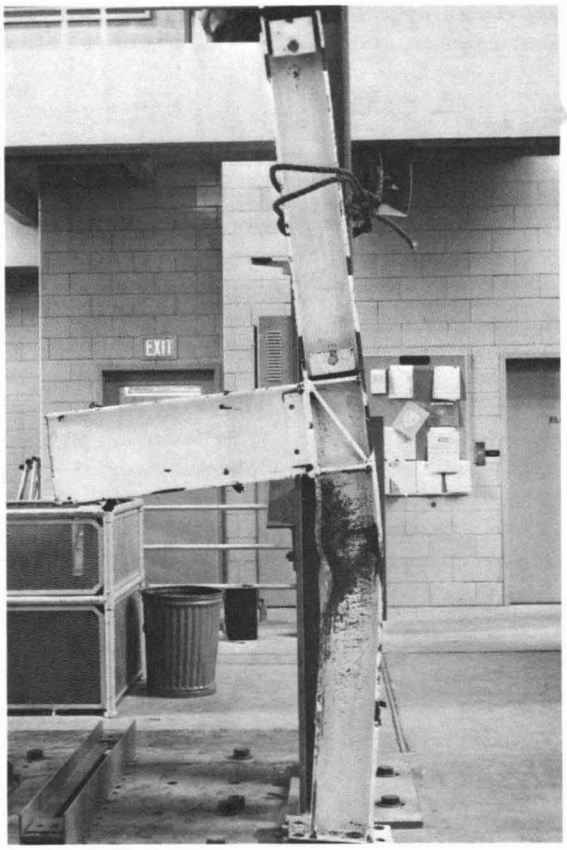

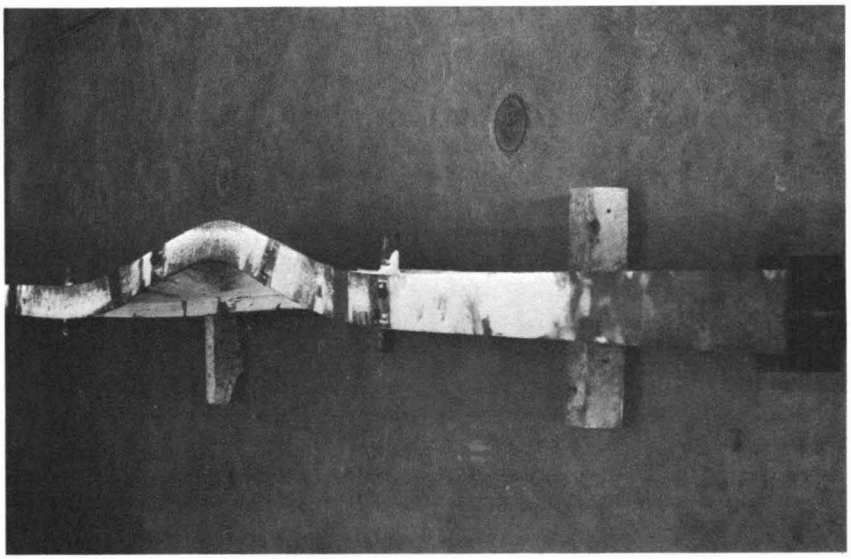

FIG. 26 DEFORMED SPECIMEN AFTER TEST RC-1

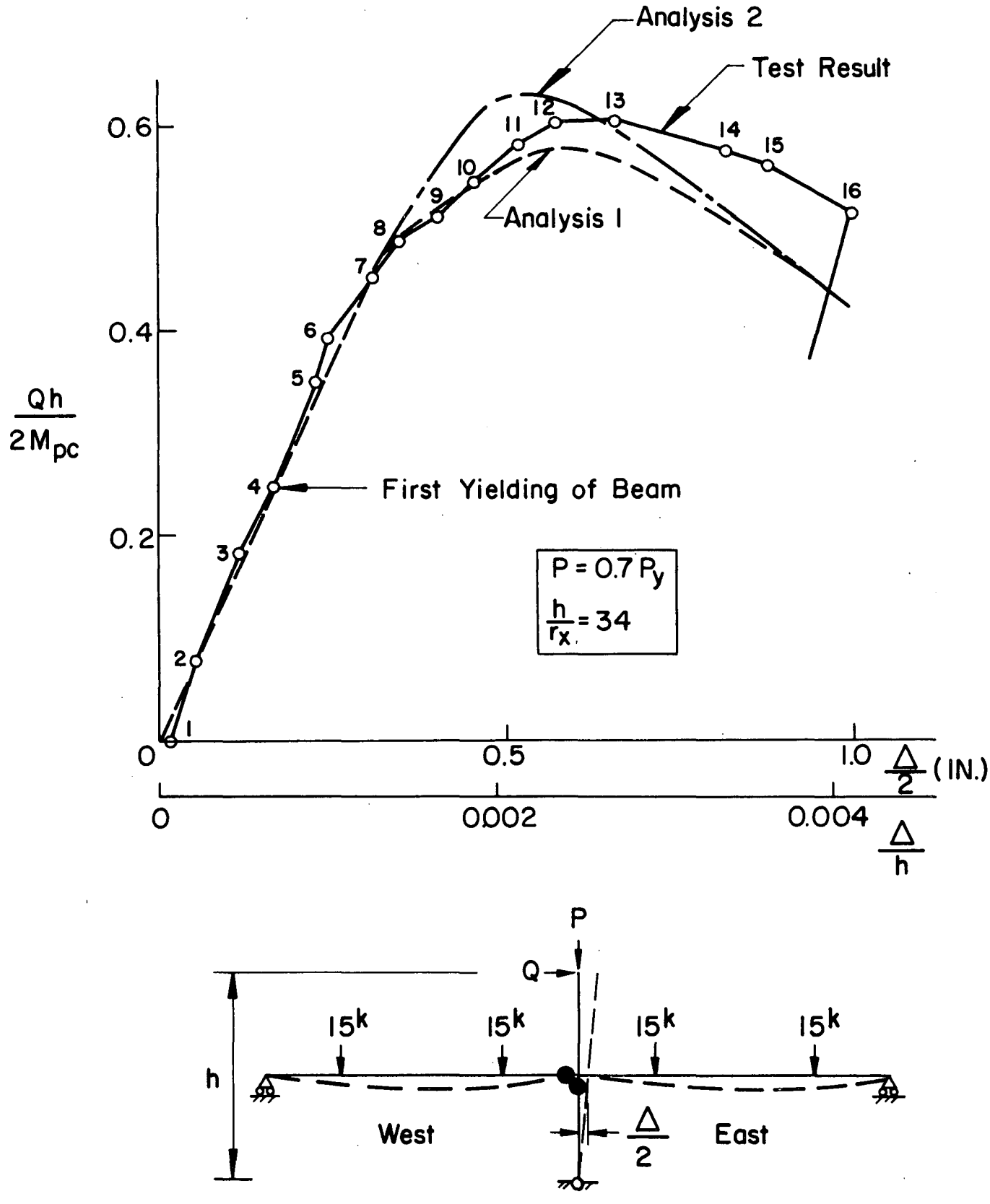

FIG. 27 LOAD DEFLECTION CURVE FOR TEST SPECIMEN RC-2

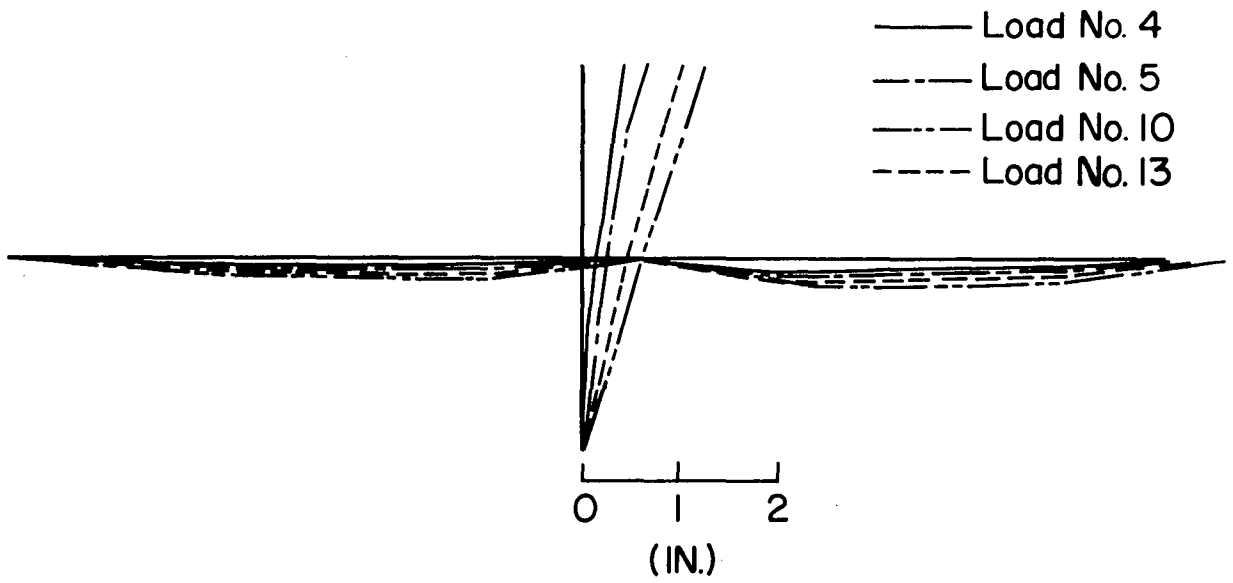

FIG. 28 DEFLECTIONS OF TEST SPECIMEN RC-2

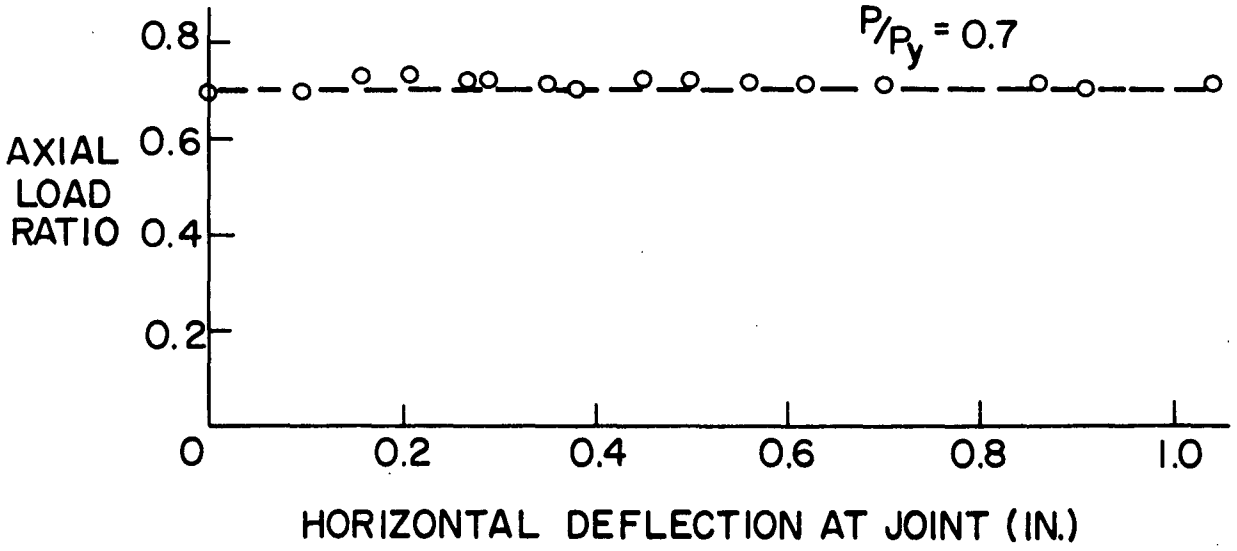

FIG. 29 VARIATION IN AXIAL LOAD RATIO IN TEST SPECIMEN RC-2

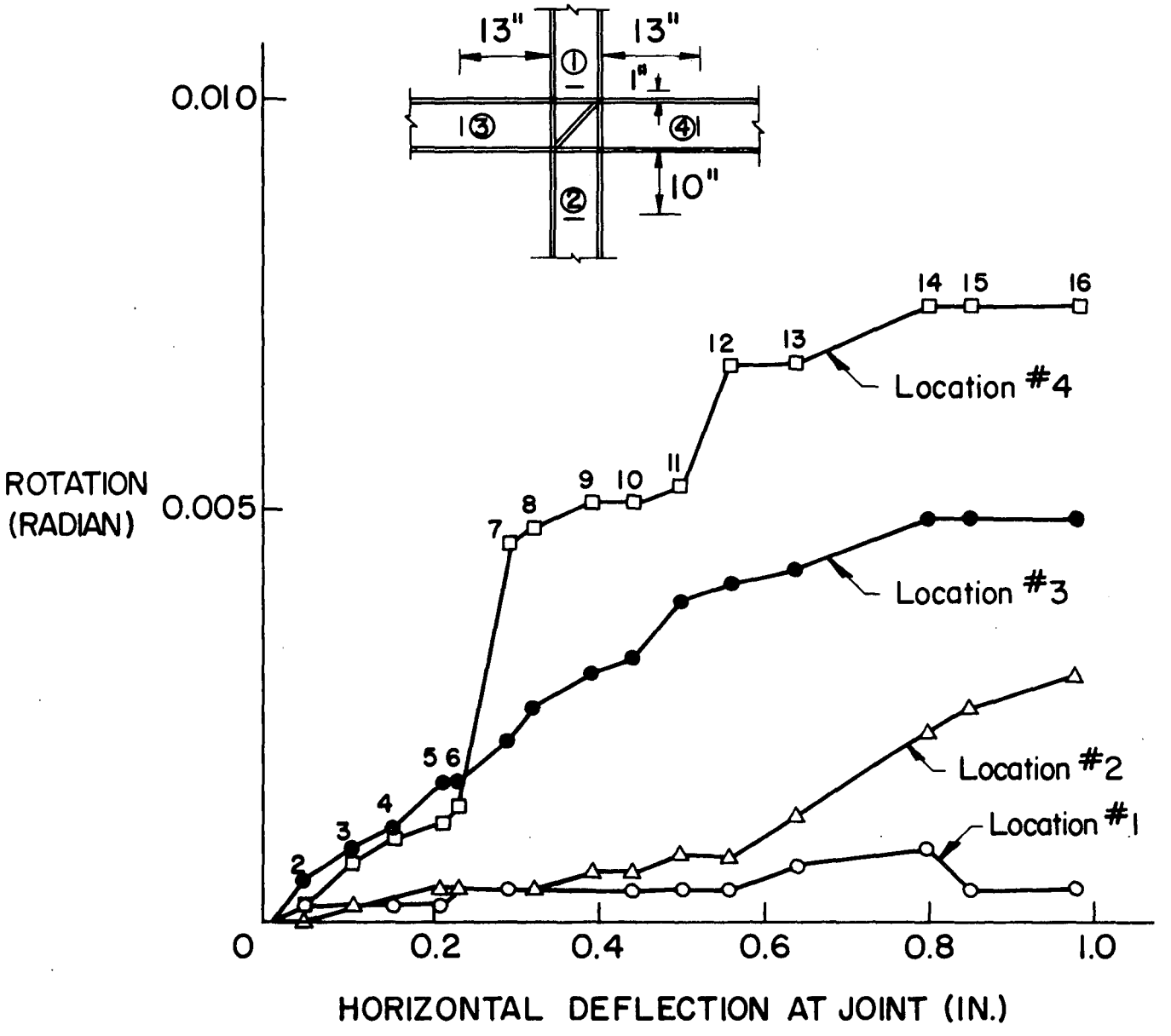

FIG. 30 ROTATIONS NEAR JOINT IN TEST SPECIMEN RC-2

FIG. 31 DEFORMED SPECIMEN AFTER TEST RC-2

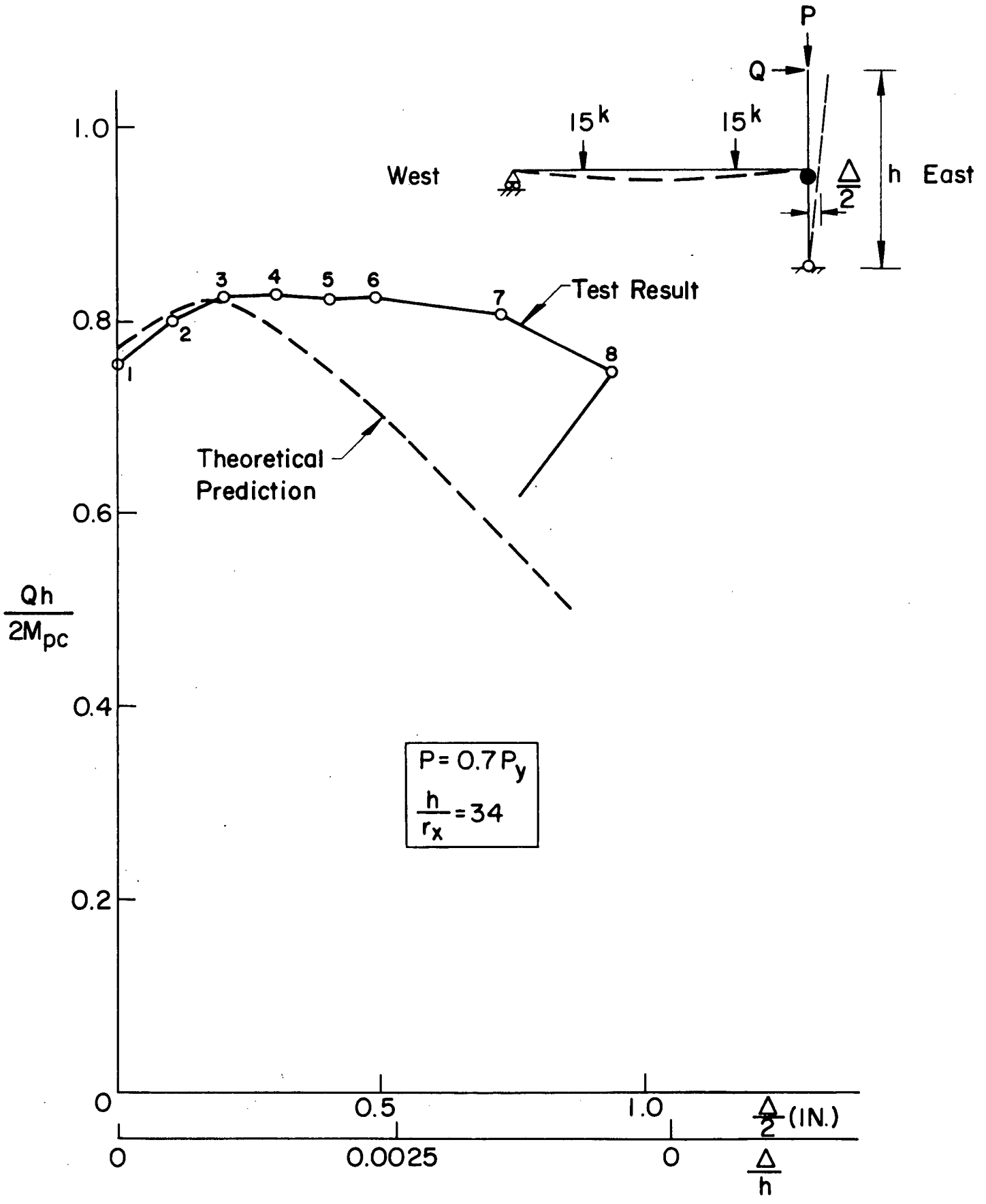

FIG. 32 LOAD DEFLECTION CURVE FOR TEST SPECIMEN RC-3

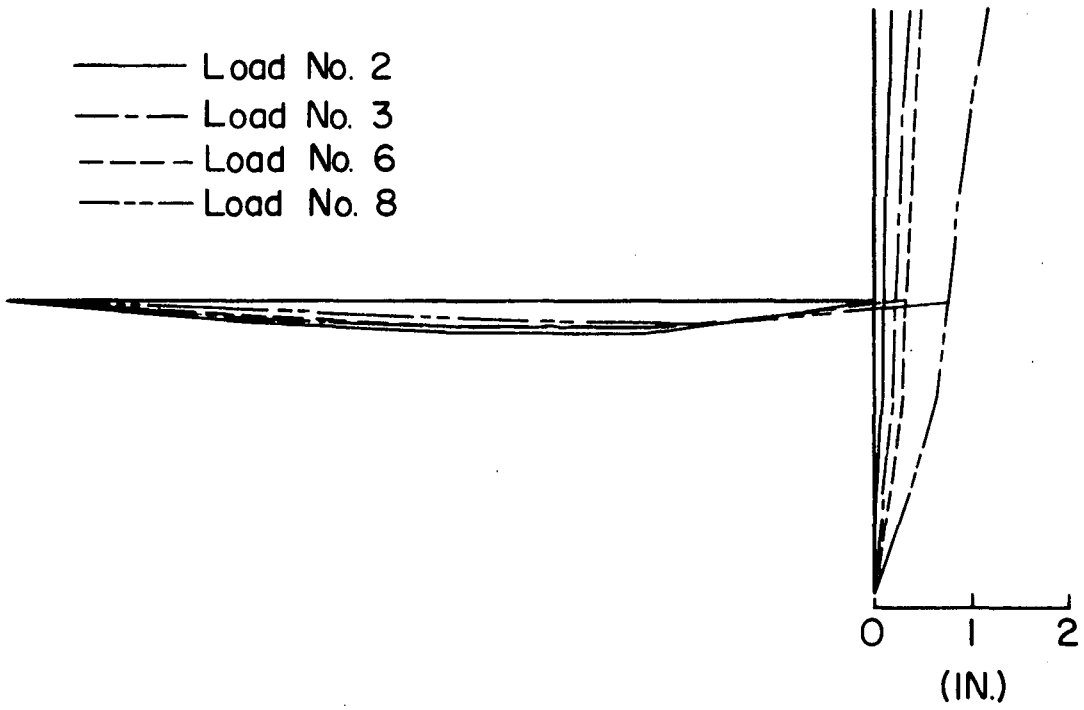

FIG. 33 DEFLECTIONS OF TEST SPECIMEN RC-3

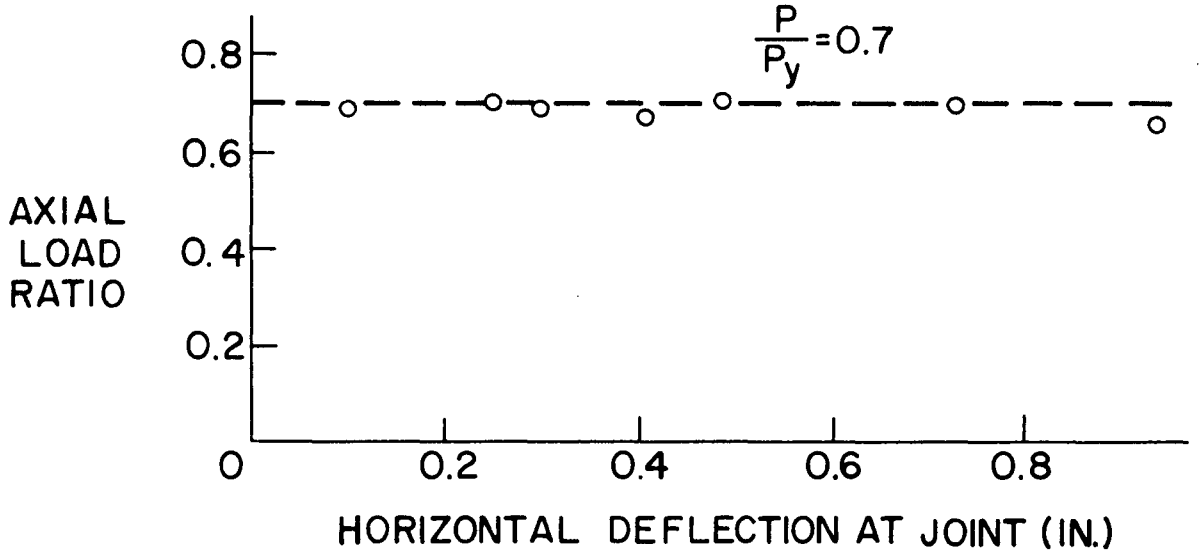

FIG. 34 VARIATION IN AXIAL LOAD RATIO IN TEST SPECIMEN RC-3

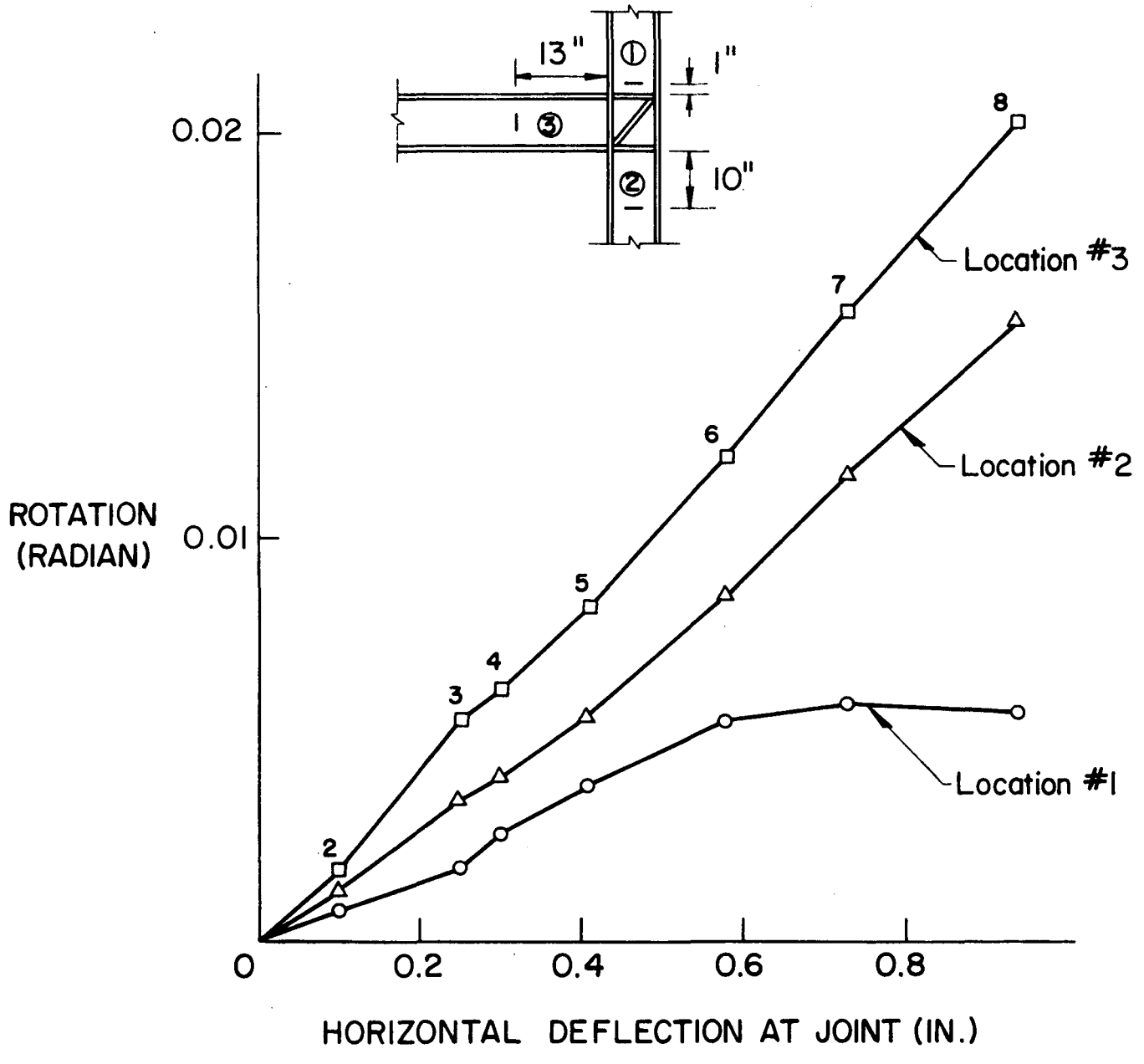

FIG. 35 ROTATIONS NEAR JOINT IN TEST SPECIMEN RC-3

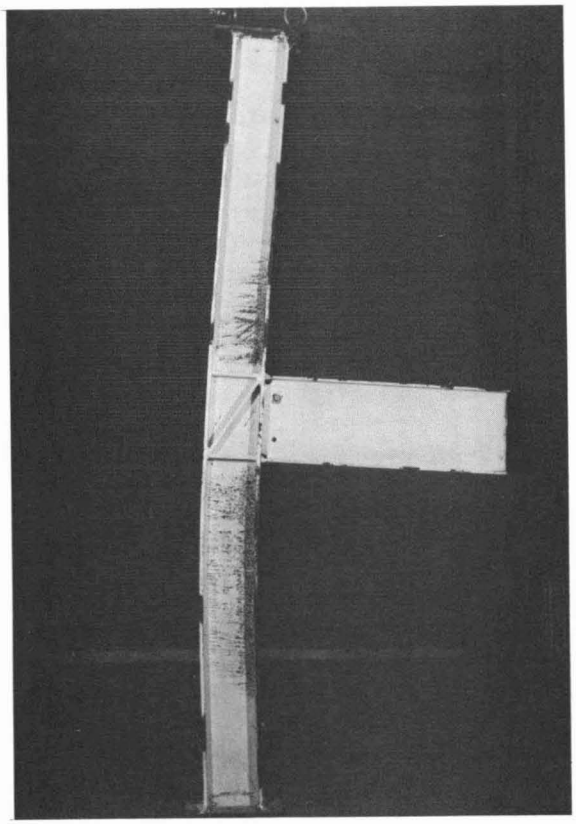

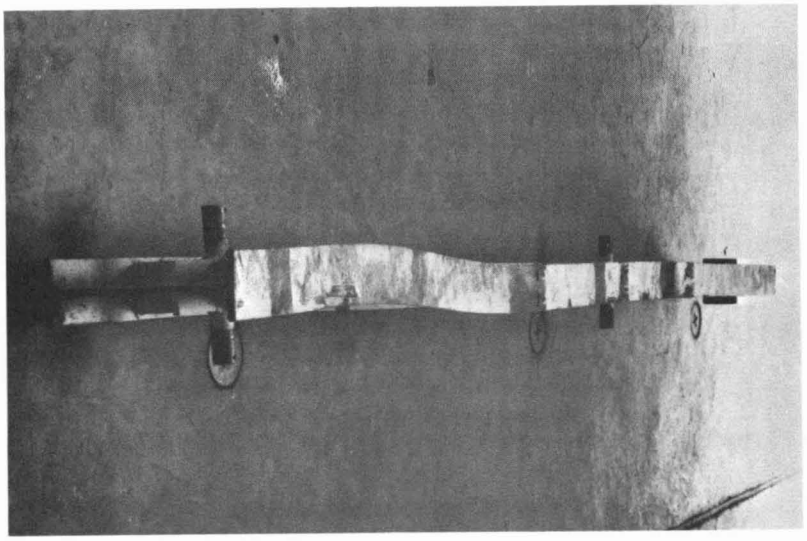

FIG. 36 DEFORMED SPECIMEN AFTER TEST RC-3

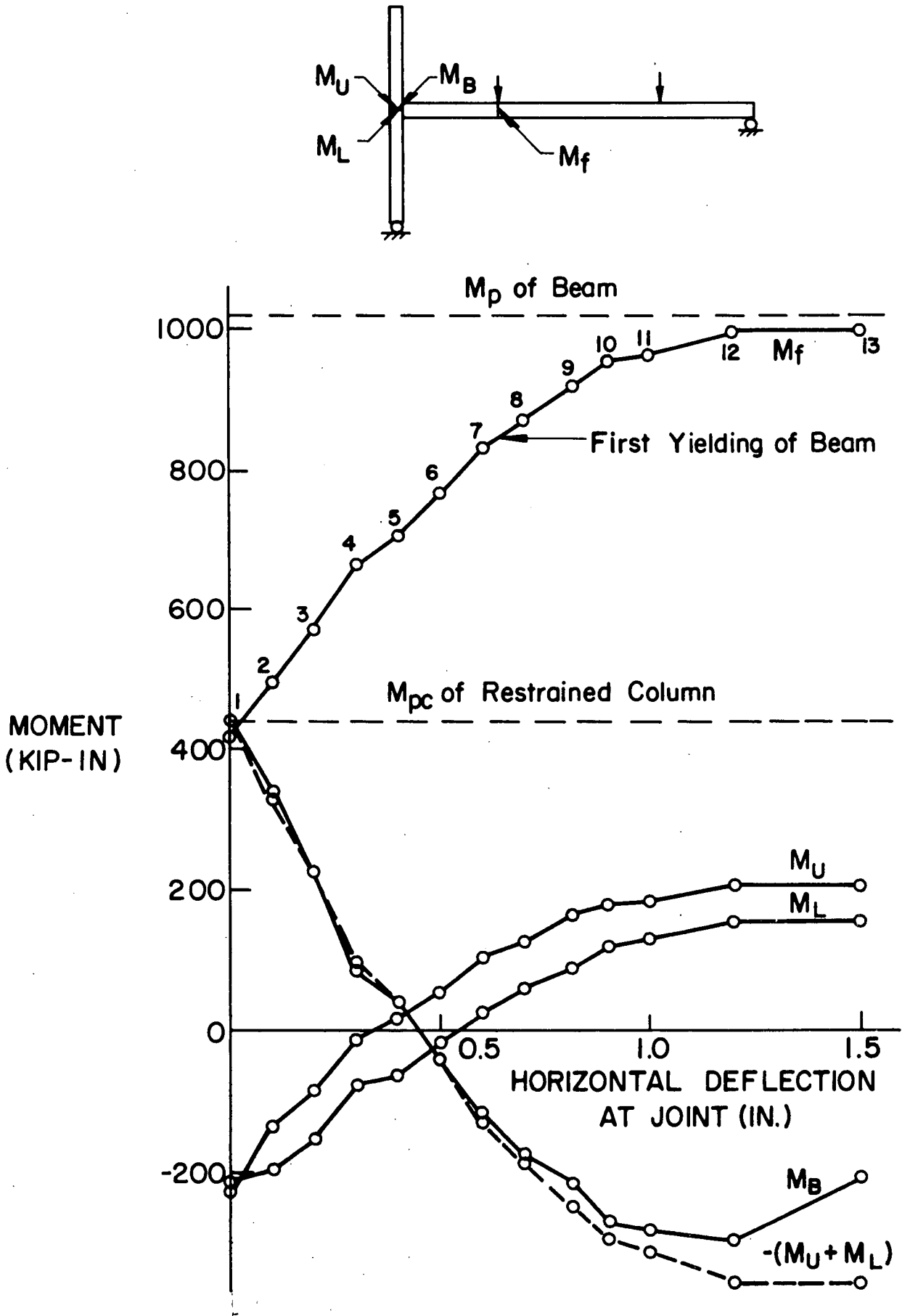

FIG. 37 VARIATION IN MOMENT IN TEST SPECIMEN RC-1

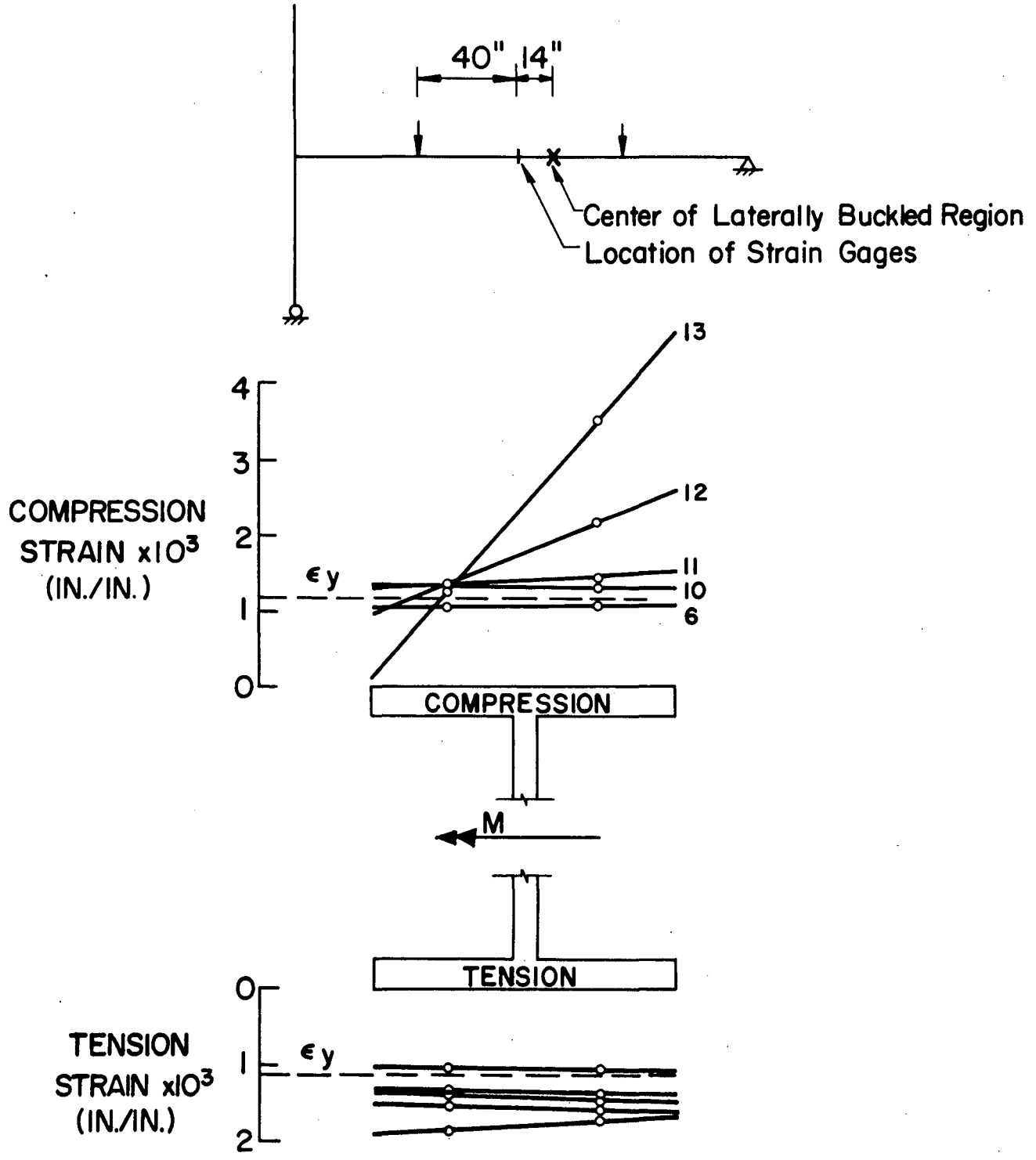

Fig. 38 STRAIN DISTRIBUTION IN BEAM FLANGES NEAR THE CENTER OF THE LATERALLY BUCKLED REGION RC-1

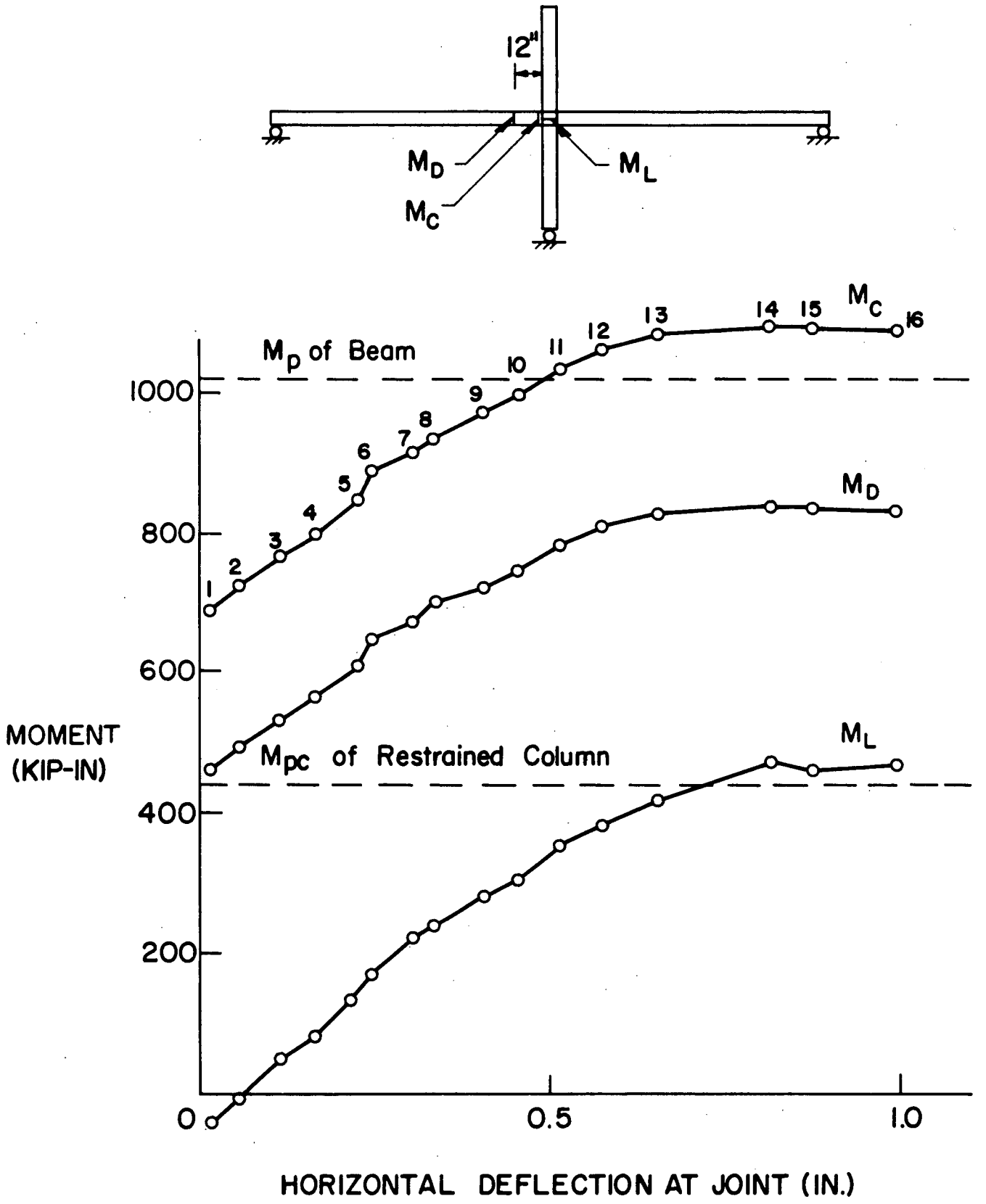

FIG. 39 VARIATION IN MOMENT IN TEST SPECIMEN RC-2

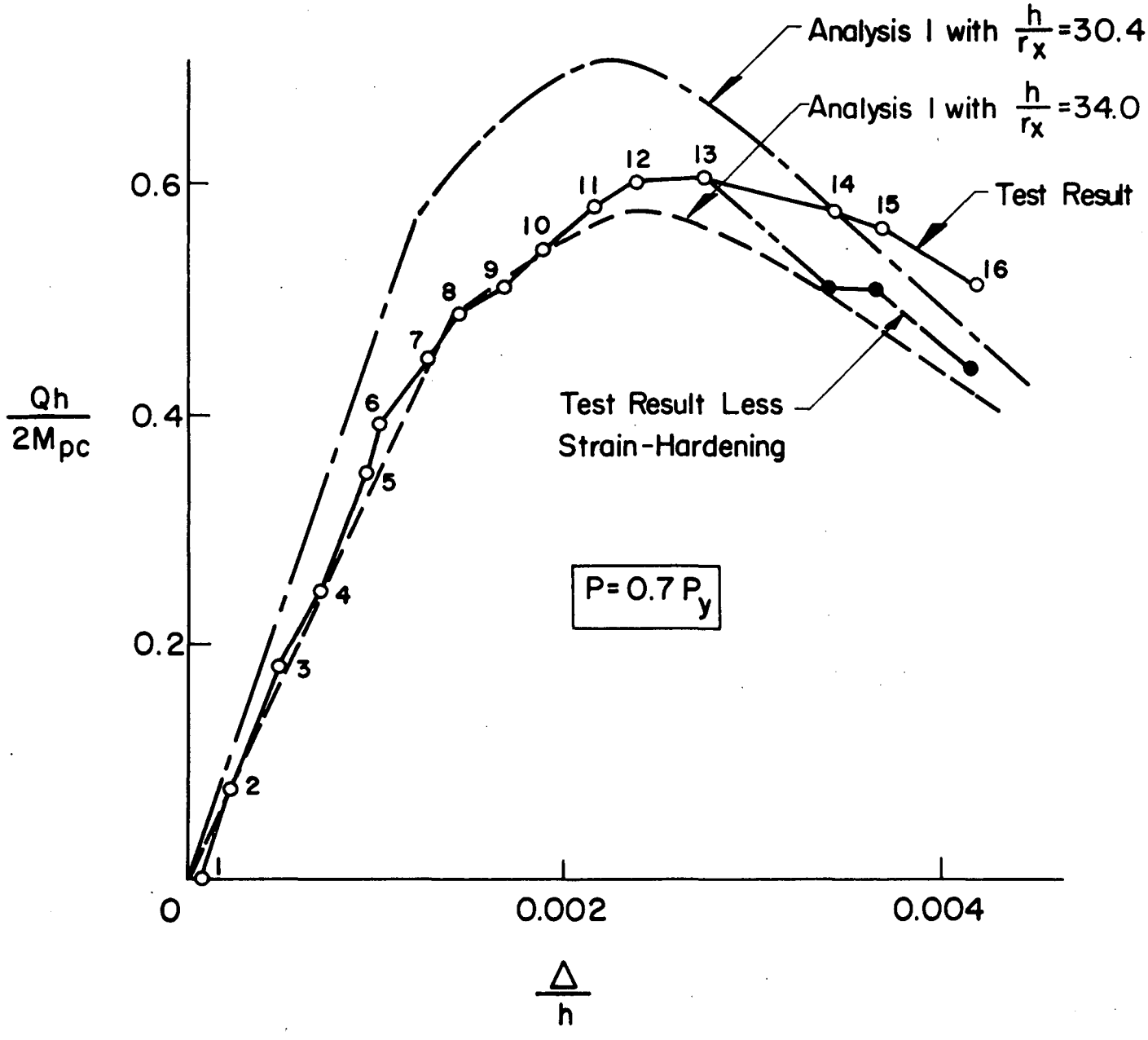

FIG. 40 COMPARISON STUDY OF TEST DATA FOR TEST SPECIMEN RC-2

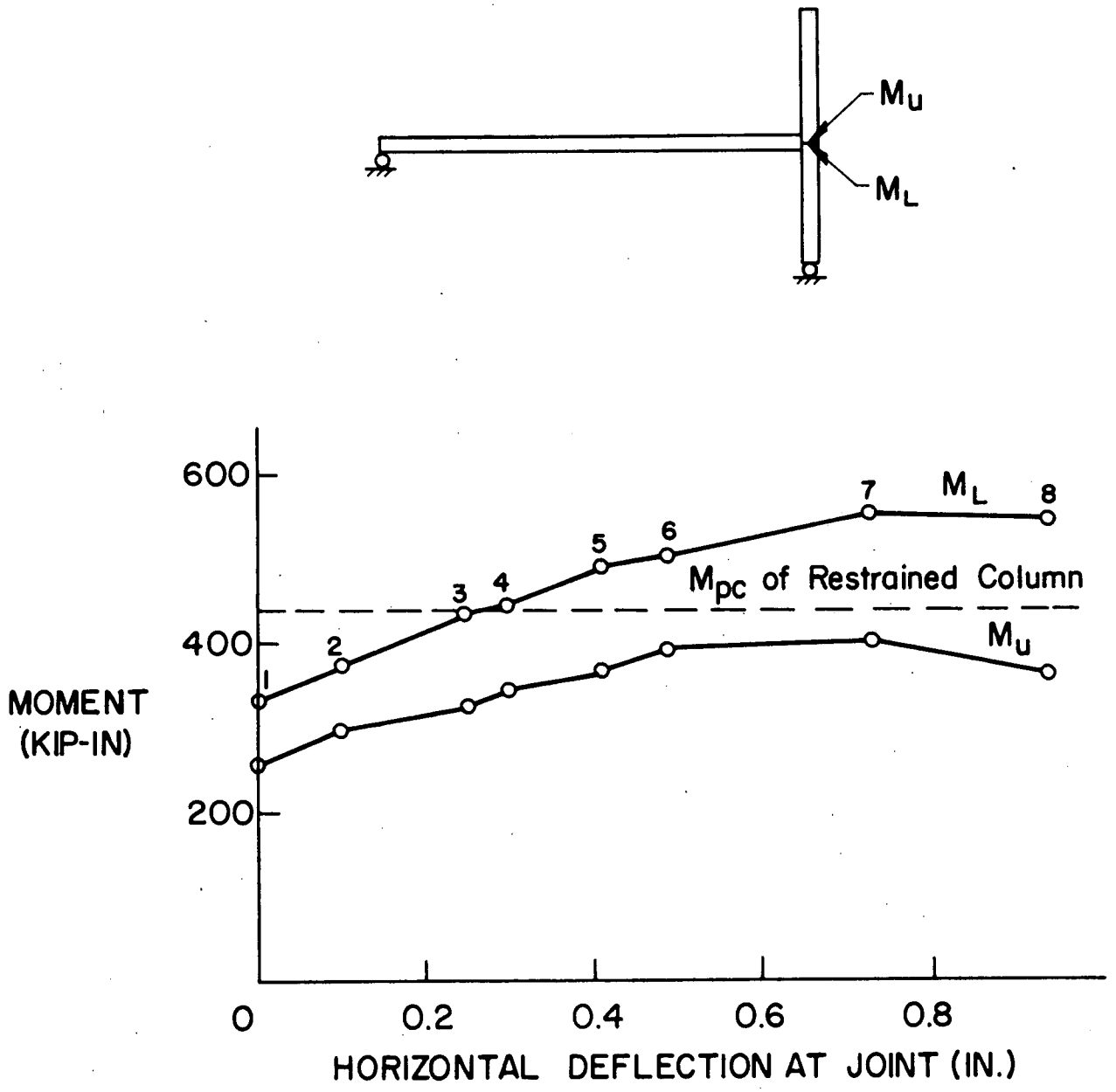

FIG. 41 VARIATION IN MOMENT IN TEST SPECIMEN RC-3

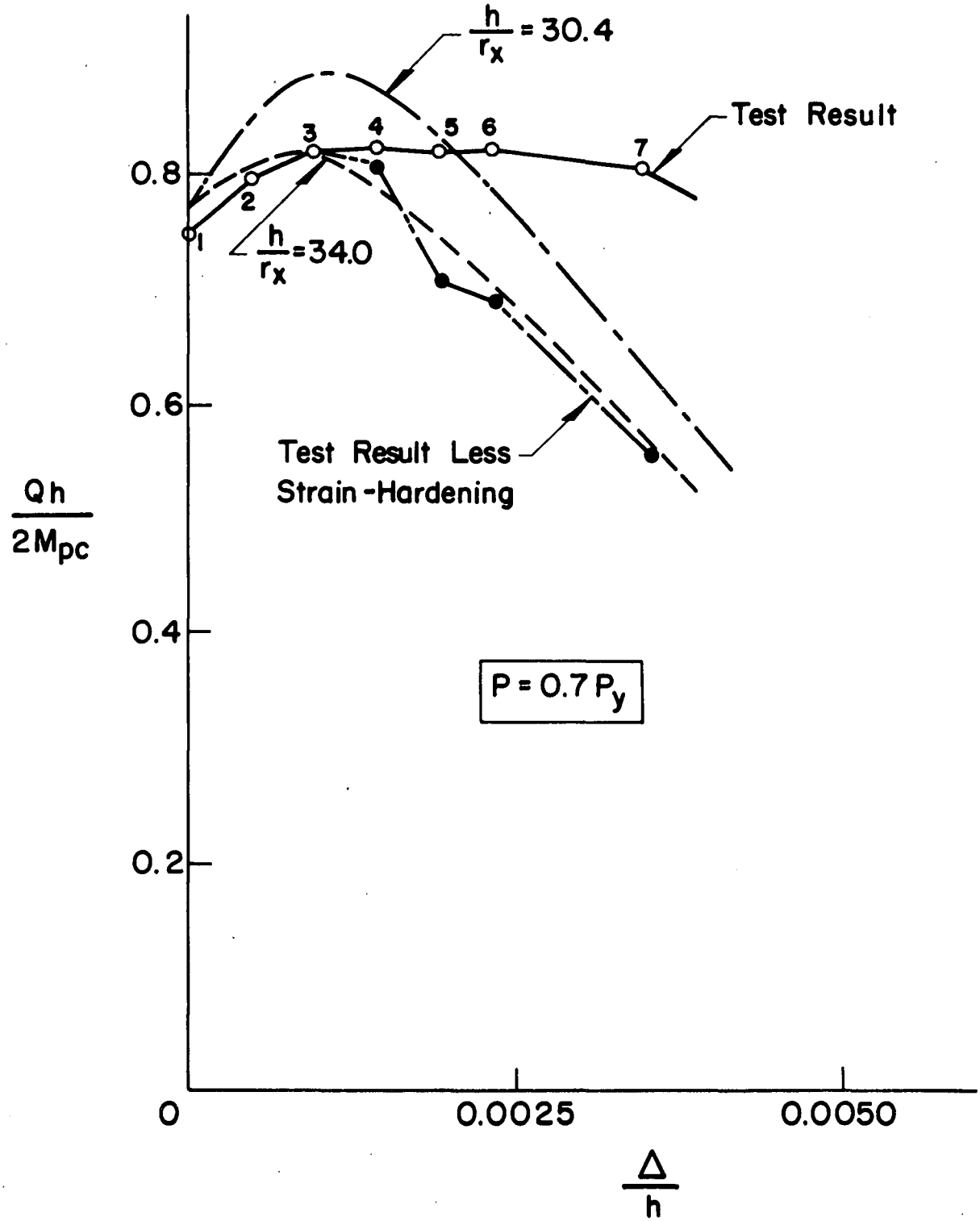

FIG. 42 COMPARISON STUDY OF TEST DATA FOR TEST SPECIMEN RC-3

11. REFERENCES

1. Daniels, J. H. and Lu, L. W.
   SWAY SUBASSEMBLAGE ANALYSIS FOR UNBRACED FRAMES, ASCE Meeting Preprint 717, Oct., 1968.

2. Daniels, J. H.
   A PLASTIC METHOD FOR UNBRACED FRAME DESIGN, AISC Engineering Journal, Vol. 3, No. 4, (October 1966).

3. Daniels, J. H.
   COMBINED LOAD ANALYSIS OF UNBRACED FRAMES, Ph.D. Dissertation, Fritz Engineering Laboratory Report No. 338.2, Lehigh University, July 1967.

4. Daniels, J. H. and Lu, L. W.
   DESIGN CHARTS FOR THE SUBASSEMBLAGE METHOD OF DESIGNING UNBRACED MULTI-STORY FRAMES, Fritz Engineering Report No. 273.54, Lehigh University, November 1966.

5. Armacost, J. O., III and Driscoll, G. C., Jr.
   THE COMPUTER ANALYSIS OF UNBRACED MULTI-STORY FRAMES, Fritz Engineering Laboratory Report No. 345.5, Lehigh University, May 1968.

6. Driscoll, G. C., Jr., Armacost, J. O., III and Hansell, W. C.
   PLASTIC DESIGN OF MULTI-STORY FRAMES BY COMPUTER, Proc. ASCE, Vol. 96, No. ST1, January 1970.

7. Levi, V., Driscoll, G. C., Jr. and Lu, L. W.
   ANALYSIS OF RESTRAINED COLUMNS PERMITTED TO SWAY, Proc. ASCE, Vol. 93, No. ST1, February 1967.

8. Kim, S. W., Daniels, J. H. and Lu, L. W.
   TECHNICAL PROPOSAL NO. 1 - RESTRAINED COLUMN TESTS, Fritz Engineering Laboratory Report No. 346.1, Lehigh University, September 1967.

9. Yarimci, E., Yura, J. A. and Lu, L. W.
   TECHNIQUES FOR TESTING STRUCTURES PERMITTED TO SWAY, Fritz Engineering Laboratory Report No. 273.40, Lehigh University, May 1966.

10. Driscoll, G. C., Jr. and others
    PLASTIC DESIGN OF MULTI-STORY FRAMES - LECTURE NOTES, Fritz Engineering Laboratory Report No. 273.20, Lehigh University, Sept. 1965.

11. Lay, M. G. and Galambos, T. V.
TESTS ON BEAM AND COLUMN SUBASSEMBLAGES, Fritz Engineering Laboratory Report No. 278.10, Lehigh University, June 1964.

12. Yarimci, E.
INCREMENTAL INELASTIC ANALYSIS OF FRAMED STRUCTURES AND SOME EXPERIMENTAL VERIFICATIONS, Ph.D. Dissertation, Lehigh University, May 1966.

13. Yu, C. K.
INELASTIC COLUMNS WITH RESIDUAL STRESSES, Ph.D. Dissertation, Lehigh University, April 1968.